POLITECNICO
MILANO 1863

SCUOLA DI INGEGNERIA INDUSTRIALE
E DELL'INFORMAZIONE

Influence of silanization and sulfur content on curing kinetics and Payne effect in silica-filled styrene-butadiene rubbers

MASTER THESIS IN
MATERIALS ENGINEERING AND NANOTECHNOLOGY
INGEGNERIA DEI MATERIALI E DELLE NANOTECNOLOGIE

Author: **Gianluca Vigani**

Student ID: 225584
Advisor: F. Briatico Vangosa
Co-advisor: C. Marano
Academic Year: 2025-2026

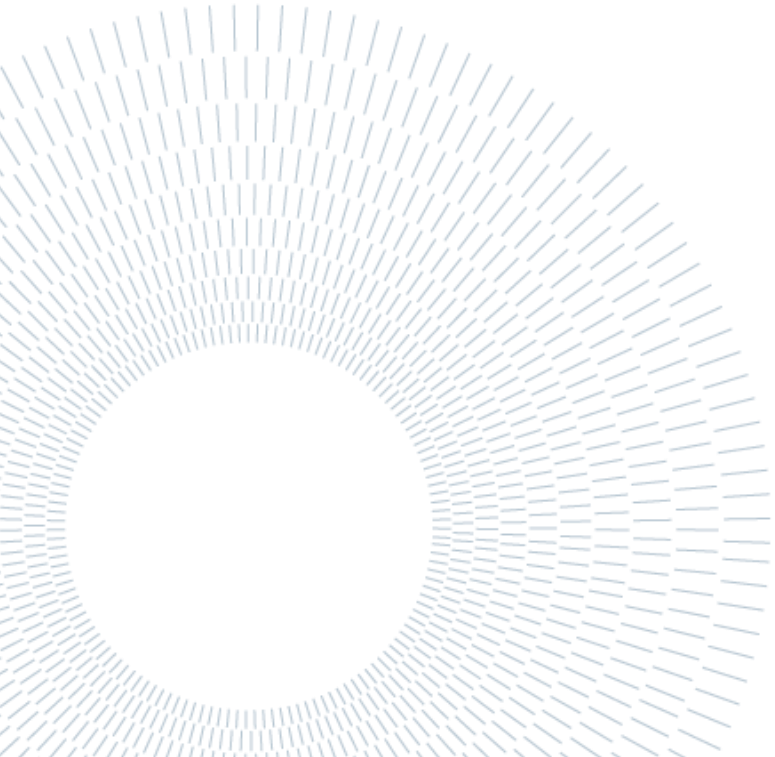

Abstract

This research investigates the influence of silanization level and sulfur content on the nonlinear viscoelastic behaviour of silica-filled styrene-butadiene rubber (SBR), with particular focus in their influence on Payne effect and on curing kinetics. The study examines compounds with varying TESPT concentrations in both uncured and cured states in order to distinguish the respective roles of the filler-filler network, the filler-rubber interface, and the chemical crosslink network. Experimental tests were carried out using a Rubber Process Analyzer operating in torsional strain-controlled mode. Curing kinetics were first evaluated under isothermal conditions to determine the dependence of it over the TESPT and sulfur content. Subsequently, large amplitude oscillatory shear (LAOS) tests were performed to analyze the strain-dependent evolution of the storage (G') and loss (G") moduli and to characterize the nonlinear mechanical response of these materials. Given the intrinsic nonlinear nature of filled rubbers, harmonic analysis techniques were employed to quantify deviations from linear viscoelastic behaviour. Fourier-based methods and Chebyshev decomposition were applied to evaluate higher harmonic contributions, while the LeBlanc-Nijman model was used to provide a parametric description of the total harmonic content evolution. The results clarify how silanization and sulfur content influence both curing behaviour and nonlinear viscoelastic response, providing a coherent interpretation of the transition from filler-dominated to matrix-dominated regimes in silica-filled SBR compounds.

Key-words: Payne effect, reinforced elastomers, silanization, curing kinetics, LAOS.

Abstract in italiano

Questa ricerca indaga l'influenza del livello di silanizzazione e del contenuto di zolfo sul comportamento viscoelastico non lineare di gomme stirene-butadiene (SBR) caricate con silice, con particolare attenzione alla loro influenza sull'effetto Payne e sulla cinetica di vulcanizzazione. Lo studio esamina mescole con differenti concentrazioni di TESPT sia nello stato non reticolato che in quello reticolato, al fine di distinguere i rispettivi ruoli della rete filler-filler, dell'interfaccia filler-gomma e della rete chimica di reticolazione. Le prove sperimentali sono state condotte utilizzando un Rubber Process Analyzer operante in modalità torsionale a deformazione controllata. La cinetica di vulcanizzazione è stata inizialmente valutata in condizioni isotermiche per determinarne la dipendenza dal contenuto di TESPT e di zolfo. Successivamente, sono state eseguite prove di taglio oscillatorio a grande ampiezza di deformazione (LAOS) per analizzare l'evoluzione dipendente dalla deformazione dei moduli di conservazione (G') e di perdita (G'') e per caratterizzare la risposta meccanica non lineare di questi materiali. Data la natura intrinsecamente non lineare delle gomme caricate, sono state impiegate tecniche di analisi armonica per quantificare le deviazioni dal comportamento viscoelastico lineare. Metodi basati sulle trasformate di Fourier e sulla decomposizione di Chebyshev sono stati applicati per valutare i contributi delle armoniche superiori, mentre il modello di LeBlanc-Nijman è stato utilizzato per fornire una descrizione parametrica dell'evoluzione del contenuto armonico totale. I risultati chiariscono come il livello di silanizzazione e il contenuto di zolfo influenzino sia il comportamento di vulcanizzazione sia la risposta viscoelastica non lineare, fornendo un'interpretazione coerente della transizione da un regime dominato dal filler a uno dominato dalla matrice nei sistemi SBR caricati con silice.

Parole chiave: Effetto Payne, elastomeri rinforzati, silanizzazione, cinetica di vulcanizzazione, LAOS.

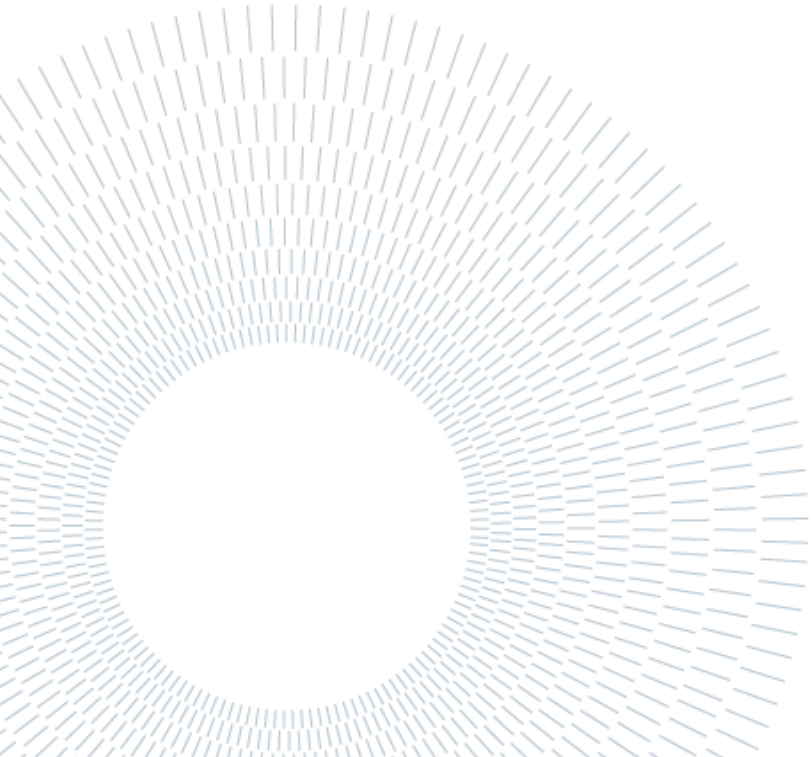

Contents

Introduction

Elastomeric materials filled with reinforcing particles are widely employed in a broad range of industrial applications, including tires and damping devices. In these applications, rubber compounds are routinely subjected to cyclic deformations over a wide range of amplitudes, frequencies, and temperatures. As a consequence, their performance is not governed solely by linear viscoelastic properties, but by complex nonlinear responses arising from the interplay between the polymer matrix, the filler phase, and their mutual interactions.

Among reinforcing fillers, silica has gained increasing importance in recent decades, particularly in "green tire" technology, due to its ability to improve rolling resistance and wet grip. However, the highly polar nature of silica surfaces leads to strong filler-filler interactions and poor compatibility with non-polar elastomers such as styrene-butadiene rubber (SBR). To overcome these limitations, silane coupling agents, most notably TESPT, are widely used to promote filler dispersion and improve filler-rubber interactions.

The present thesis focuses on the nonlinear viscoelastic response of silica filled styrene-butadiene rubber (SBR) compounds, with particular attention to the role of silane coupling agents in governing filler-related reinforcement mechanisms.

Despite the extensive industrial use of silica-silane systems, the relationship between coupling agent content, filler network structure, and nonlinear viscoelastic response remains only partially understood. In particular, the Payne effect, commonly observed as a strong dependence on the strain amplitude of the storage and loss moduli under oscillatory deformation, provides a macroscopic manifestation of the underlying microstructural evolution of filled elastomers. While the origin of this phenomenon is well established, its quantitative interpretation is not completely understood, especially when considering the specific influence of the coupling agent concentration on the evolution of nonlinear behaviour in both the uncured and cured states of the material, together with its effect on curing kinetics and crosslink network development.

To address these aspects, a systematic experimental study was carried out using a Rubber Process Analyzer (RPA), which enables the investigation of the viscoelastic response of rubber compounds under controlled oscillatory shear conditions over a wide range of strain amplitudes. Compounds with different levels of silane coupling agent were examined both in the uncured and cured states, allowing the investigation

of curing kinetics and the separation of physical reinforcement effects from those associated with the chemical crosslink network.

The nonlinear mechanical response was investigated through amplitude sweep experiments, with particular emphasis on the evolution of the storage and loss moduli and on the emergence of nonlinear features beyond the linear viscoelastic regime. The experimental results were analyzed using different approaches in order to characterize the strain-dependent response, the evolution of curing and to understand more about the mechanisms behind the Payne effect.

Overall, this work aims to contribute to a deeper understanding of the structure-property relationships in silica filled elastomers, highlighting how coupling agent concentration affect the curing state and the nonlinear viscoelastic behaviour. Through theoretical and experimental methods, the study contributes to the broader knowledge of this critical phenomenon in material science, with potential implications for its practical applications.

1 Theoretical background

The subsequent sections provide an in-depth description of the structure and behaviour of elastomers, together with an exploration of the governing principles of viscoelastic materials as characterized by Dynamic Mechanical Analysis (DMA). Attention then shifts to the nonlinear response of filled elastomers under oscillatory deformation. A structured overview of the principal analytical methods used to detect and quantify nonlinearity is first provided, including harmonic-based approaches for interpreting distorted stress signals. The discussion then focuses on the Payne effect as the macroscopic manifestation of strain-dependent softening in filled elastomers. Finally, the LeBlanc-Nijman model is introduced as a quantitative framework to describe the evolution of higher harmonic contributions and to interpret the transition from filler-dominated to matrix-dominated behaviour.

1.1. Elastomers

Elastomers are a class of polymeric materials characterized by their ability to undergo large reversible deformations [1]. This unique mechanical behavior originates from their molecular architecture, consisting of long, flexible polymer chains arranged in a highly disordered, randomly coiled configuration and interconnected through a three-dimensional network [1] [2]. At equilibrium, this structure corresponds to a state of high configurational entropy.

Since elastomers operate at temperatures well above their glass transition temperature (Tg), chain mobility is high, allowing the macromolecules to move and reorient easily under applied stress. When a mechanical load is imposed, the chains progressively align along the deformation direction, leading to large strains at relatively low applied stresses. Once the load is removed, the presence of network junctions prevents the chains from slip or disentangle and enables the entropic recovery of the disordered equilibrium configuration, so that the imposed deformation is fully recovered.

Elastomeric behaviour is intrinsically associated with the formation of a three-dimensional network connecting the polymer chains. In the absence of such a network, the rubber behave as an highly viscous material with limited mechanical strength and poor resistance to flow. For this reason, before being employed in industrial applications, rubber compounds undergo physical and chemical processes aimed at

stabilizing their molecular structure and enhancing their mechanical performance. One of the most significant processes in this regard is vulcanization, which involves the chemical creation of covalent network junctions through the insertion of crosslinks between polymer chains. Typically it consists in heating the rubber with sulfur-based vulcanizing agents which can form sulfur bridges between macromolecules [1] [3], transforming these highly viscous liquids into solid-like materials with outstanding elastic recovery.

Although a permanent network is required for elastomeric behaviour to occur, the mechanical response of the un-crosslinked material is also of considerable interest, particularly during its processing into the final shape, after which curing is carried out to obtain the consolidated elastomeric product.

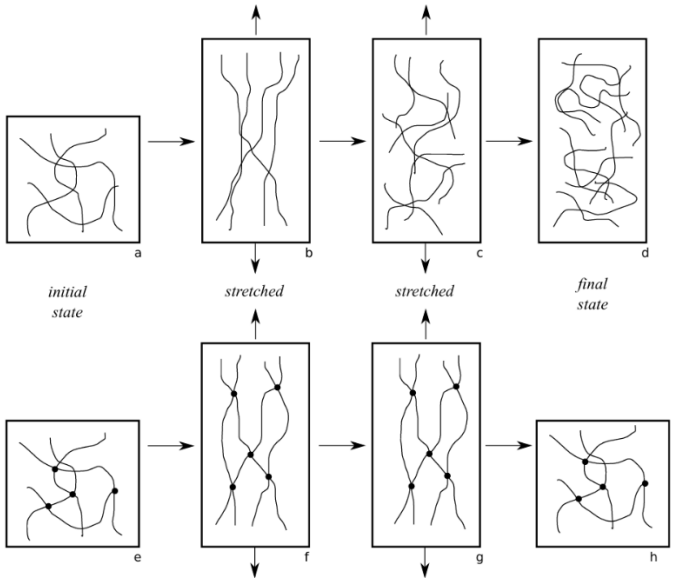

Figure 1.1. Effect of stretching on a non-vulcanized (above) and a vulcanized (below) elastomer

The material response to an externally applied strain differs significantly between the uncured and cured states, as it is governed by distinct structural mechanisms, illustrated in Figure 1.1. In the uncured state, polymer chains are free to move relative to one another, being constrained only by van der Waals interactions and chain entanglements. At low deformations, uncured rubber compounds behave as viscoelastic solids, dominated by chain entanglements. As strain increases, chains progressively align and disentangle, leading to irreversible deformation. Once the load is removed, having been plastically deformed, the material doesn't return to its original configuration.

In the cured state, by contrast, the mechanical response is dominated by the covalent crosslink network that permanently connects the polymer chains. As deformation

increases, chains again tend to align along the loading direction, but the presence of crosslinks restricts relative chain mobility and prevents disentanglement. Consequently, even after large deformations, the applied strain can be entirely recovered once the load is removed, and the material returns to its original shape.

1.2. Reinforced elastomers

Even if the elastomers display the ability to recover the original equilibrium conformation after high strains, they are so compliant that their use in several application would be impractical. Therefore, in the rubber industry many types of fillers with different characteristics and activities are used [4] [5] [6] [7] [8] to enhance their mechanical and thermal performance increasing both the modulus and the deformation at break. The reinforcing effect of the filler mainly depends on the size of the particles and their distribution in the elastomer matrix, as well as on the specific surface area and chemical and physical nature of the filler [9].

Beyond the purely mechanical reinforcement, fillers also strongly affect the processing behavior and the curing kinetics of rubber compounds. Their presence modifies the course and efficiency of vulcanization, as the filler surface can interact with the curing system, leading to heterogeneous crosslink distributions and, in some cases, to a reduction of the effective crosslink density [10]. These effects are particularly relevant for highly polar fillers such as silica, whose surface chemistry plays a central role in determining both the final network structure and the macroscopic mechanical response of the vulcanizate.

Among reinforcing fillers, amorphous precipitated silica has gained a dominant role in modern rubber technology, especially in applications such as “green tires”, where a favorable balance between rolling resistance, wet grip, and abrasion resistance is required. Silica combines a high specific surface area with a surface rich in silanol (Si-OH) groups [11] [12], which makes it highly active but also intrinsically polar. This polarity leads to strong filler-filler interactions through hydrogen bonding, promoting aggregation and the formation of rigid [10], highly connected filler networks that are difficult to disperse homogeneously in non-polar elastomers such as SBR.

At the same time, the polarity mismatch between the hydrophilic silica surface and the hydrophobic rubber matrix results in weak intrinsic filler-rubber interactions [13]. As a consequence, silica-filled compounds are characterized by poor compatibility, high compound viscosity. Further, unfavorable curing behaviour can occur when no surface modification is applied, since its surface can adsorb accelerators for curing reaction, which deteriorates their effectiveness and consequently results in the extension of the vulcanization time and a potential reduction in the crosslink density of the vulcanizates [14] [15].

To overcome these limitations, various strategies [16] [17] [18] [19] [20] [21] have been developed to improve the silica-rubber interaction. Among them, the use of bifunctional organosilane coupling agents represents the most widely adopted and industrially relevant approach. Silanes such as bis[3-(triethoxysilyl)propyl] tetrasulfide (TESPT) are capable of reacting with the silica surface while simultaneously participating in the sulfur curing chemistry, reducing filler-filler aggregation, improving dispersion, and strengthening filler-rubber interactions [19] [22]. This dual action directly impacts the microstructure of the filled compound and – consequently – its mechanical and dynamic properties.

Beyond classical descriptions based on hydrodynamic reinforcement and filler-filler networking, recent studies have emphasized the central role of the filler-rubber interphase in controlling the mechanical response of filled elastomers [23]. In this context, Huang et al. [24] proposed a structural model that explicitly links the reinforcing effect of silica to the formation of a multiscale filler-rubber entanglement network mediated by bound rubber layers.

According to this framework, as illustrated in Figure 1.2 and Figure 1.3, the filler-rubber interface is composed of distinct populations of polymer chains, commonly classified as tightly bound rubber, loosely bound rubber, and free or entrapped rubber. Tightly bound rubber is strongly immobilized at the filler surface through specific interactions, such as hydrogen bonding in the case of silica, while loosely bound rubber is physically adsorbed (mainly van der Waals forces [25] [26]) or entangled with the tightly bound layer. These interfacial polymer chains can act as bridges between adjacent filler aggregates [27], enabling the formation of extended filler-rubber entanglement networks.

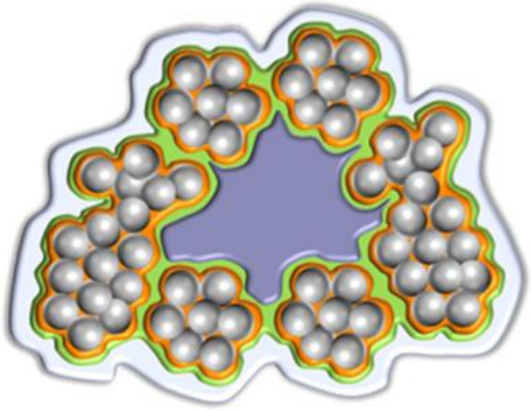

Figure 1.2 Representation of the model introduced by Huang et all. (2023)

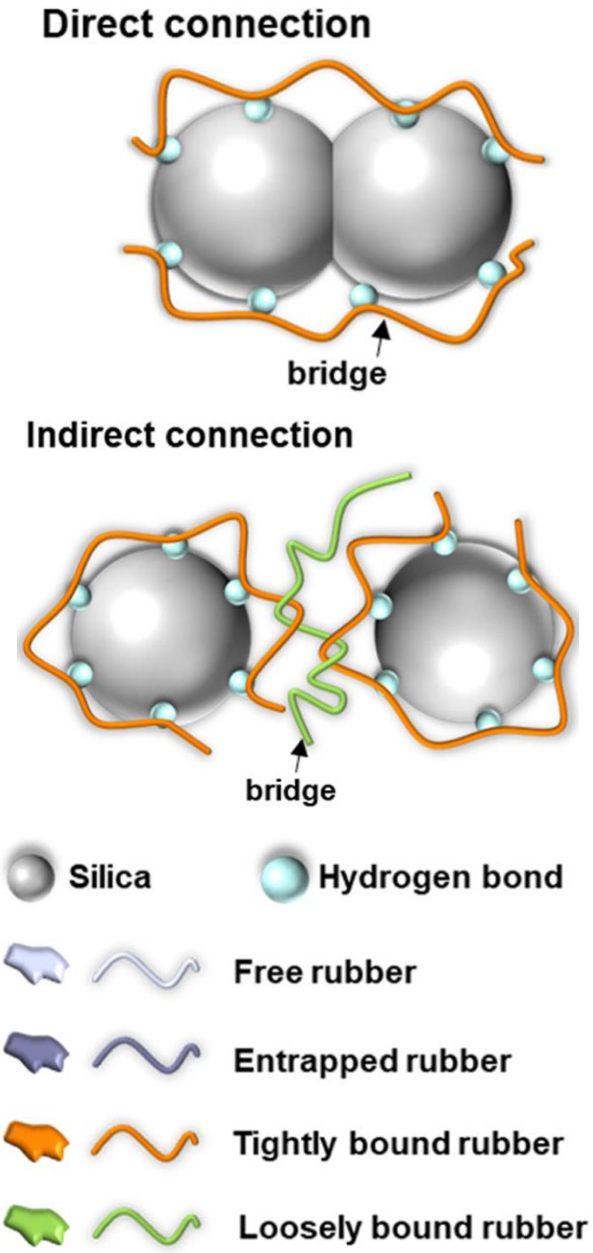

Figure 1.3 Description of the model introduced by Huang et all. (2023)

The structural continuity and mechanical stability of these networks depend not only on the amount of bound rubber, but also on the filler morphology, surface chemistry, and dispersion state. In particular, Huang et al. [24] showed that fillers capable of forming homogeneous, interconnected entanglement networks exhibit enhanced nonlinear mechanical responses, even when the absolute quantity of tightly bound rubber is relatively low. Conversely, systems characterized by large amounts of bound rubber localized on isolated aggregates tend to form heterogeneous and mechanically fragile networks.

Within this perspective, the reinforcement of filled elastomers emerges as the combined result of rigid filler inclusions, filler-filler contacts, and filler-rubber entanglement networks, whose structure evolves under applied deformation. The progressive breakdown and rearrangement of these networks under oscillatory strain provide a direct microstructural basis for nonlinear viscoelastic phenomena.

Understanding how these structural features develop and how they respond to applied strain requires experimental techniques capable of probing the material under controlled deformation conditions. In this context, dynamic mechanical analysis provides a powerful framework to investigate the viscoelastic response of filled elastomers.

1.3. Dynamic mechanical analysis

Dynamic Mechanical Analysis (DMA) is an important experimental method for characterizing the viscoelastic behaviour of polymers, which analyzes the material's steady-state response to an oscillatory deformation. In a standard DMA test a sinusoidal shear strain (or in some instance stress) is applied to a specimen:

$$\gamma(t) = \gamma_0 \sin(\omega t) \tag{1.1}$$

where γ_0 represents the shear strain amplitude, ω the angular frequency and t is the time.

A perfectly elastic material following Hooke's law (eq. 1.2), would respond in phase with the applied strain (eq. 1.1) , while, a viscous fluid, following the Newton's law (eq. 1.3), would respond in phase with the strain rate, therefore it exhibits a phase delay of $\pi/2$ with respect to the sinusoidal strain (eq. 1.1).

$$\tau = G\gamma \tag{1.2}$$

$$\tau = \eta \frac{d\gamma}{dt} \tag{1.3}$$

For a linear viscoelastic material the shear stress oscillates sinusoidally with the same angular frequency, but with a phase angle δ, arising from the coexistence of an elastic component (τ') and a viscous component (τ''), between 0 and $\pi/2$, with the first component, in phase with the strain, representing the material's ability to store energy elastically (eq. 1.4) and the latter, with $\delta = \pi/2$, representing its ability to dissipate energy (eq. 1.5).

From these components, two materials properties can be derived, G' (eq. 1.4), the storage modulus and G'' (eq. 1.5), the loss modulus:

$$G'(\omega) = \frac{\tau'}{\gamma_0} = \frac{\tau_0 \cos(\delta)}{\gamma_0} \tag{1.4}$$

$$G''(\omega) = \frac{\tau''}{\gamma_0} = \frac{\tau_0 \sin(\delta)}{\gamma_0} \tag{1.5}$$

Also the complex modulus G^* (eq. 1.6), representing the overall resistance to deformation, and the loss tangent $tan(\delta)$ (eq. 1.7), an index of the damping characteristics of the material and expressing the relative dominance of viscous to elastic behaviour, can be derived:

$$G^*(\omega) = G'(\omega) + iG''(\omega) \quad 1.6$$

$$\tan(\delta(\omega)) = \frac{G\prime(\omega)}{G\prime\prime(\omega)} \quad 1.7$$

All informations explained above are referred to [28], [29] and [1].

1.4. Lissajous plots

The first step in any in-depth analysis of the stress responses to oscillatory shearing usually is a visual investigation of all the Lissajous-Bowditch curves, which plot two oscillating signals against each other: the instantaneous stress $\tau(t)$ versus the instantaneous strain $\gamma(t)$. By looking at these plots it's possible to follow the evolution of the material response and the level of nonlinearity during the performed test.

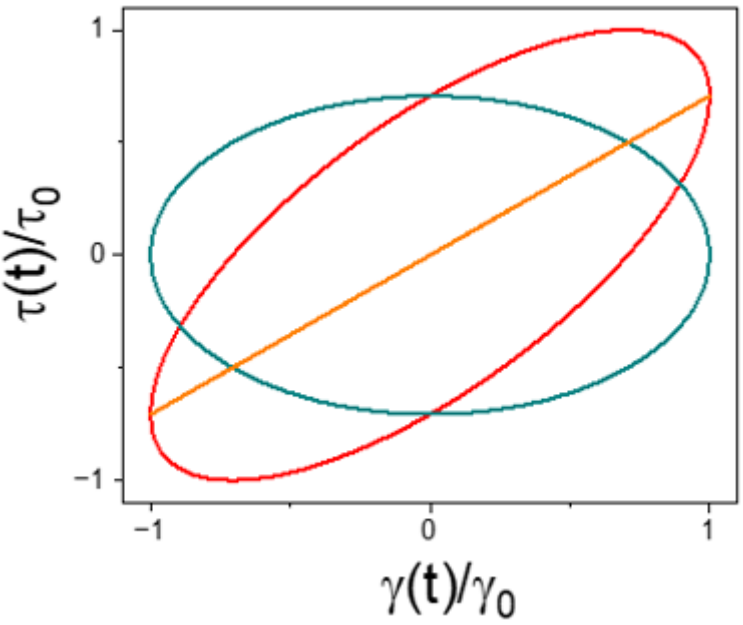

Figure 1.4 Lissajous-Bowditch plots for an ideal elastic (orange), a viscous (green) and a viscoelastic (red) material

A schematic representation of the Lissajous plots for ideal elastic, viscous and viscoelastic materials is shown in Figure 1.4. For purely elastic materials the stress response is expected to be completely in phase ($\delta = 0$) with the applied deformation, as a result the Lissajous plot is a line with the slope of G', which coincides with the

shear modulus of the material. For purely viscous materials the response is expected to be completely out of phase ($\delta = \pi/2$) resulting in an ellipse aligned with the coordinate axis for the Lissajous plot.

Since polymeric materials are viscoelastic ($0 < \delta < \pi/2$), the Lissajous plot in the linear region is expected to be an ellipse with axis tilted with respect to the coordinate axis. Any deformation from this shape would be the evidence of nonlinearity: this method therefore provides different informations, like the onset of nonlinearity, just by looking at the curves.

1.5. Linear-nonlinear dichotomy

Many industrial processes associated with polymeric materials cannot be fully described by steady shearing flow, or by linear viscoelastic deformations constrained by small amplitude oscillatory shear (SAOS) flow. This is because most polymeric materials experience large and rapid deformations during processing and application. To simulate industrial processing conditions, large-amplitude oscillatory shear (LAOS) is usually applied, since it is a test method that can investigate the nonlinear viscoelastic behaviour.

A rheological response is said to be linear if the stress-strain relations can be described by linear differential equations with constant coefficients. In the case of oscillatory shearing, where a strain is imposed sinusoidally, linearity means that a sinusoidal response with amplitude-independent coefficients is registered, sometimes with some phase shift. Therefore when the response to a sinusoidal strain is not sinusoidal.

While at small amplitudes the material's response is linear and characterized by the viscoelastic moduli G' and G'' [30], as soon as the strain amplitude increases, the response enters a nonlinear viscoelastic regime, in particular what can be usually observed in the filled-rubber case, particularly after vulcanization, is a nonlinearity characterized by a sinusoidal response, distinctly lacking higher order harmonics [31] [32] [33] [34] [35] but with amplitude-dependent coefficients. This phenomenon has been called the "linear-nonlinear dichotomy" of the Payne effect [31], and it has also been referred to as the "harmonic paradox" of filled rubbers. This absence of higher harmonics in filled rubber is evident when examining the ratio of Fourier coefficients: third harmonic response relative to the first in Figure 1.5.

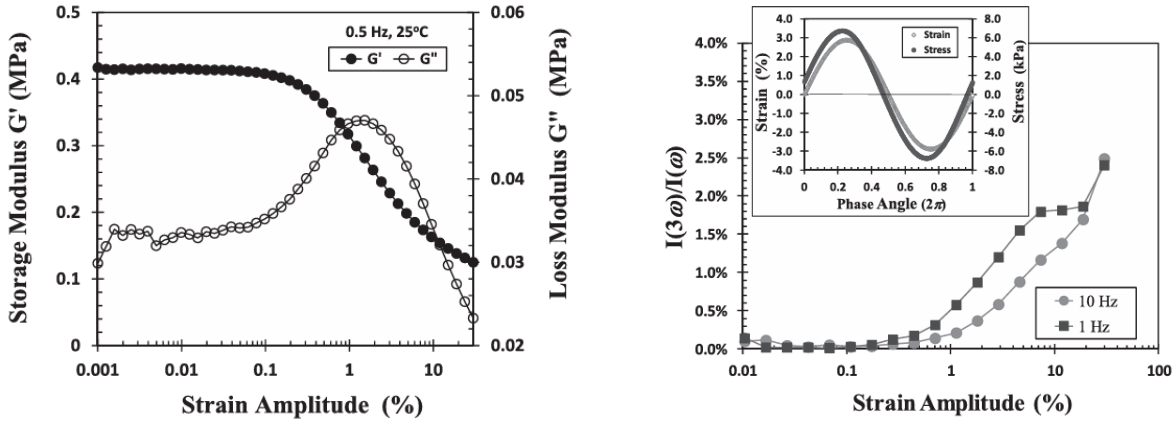

Figure 1.5. Dependence of G' and G'' (on the left) and of the ratio of first and third harmonics (on the right) on strain amplitude. The test material: SBR-CB rubber. [30]

This "linear nonlinear dichotomy" ensures that the standard deconvolution of experimental torque and phase offset in terms of G' and G'' will still be appropriate, although the γ_0-dependent G' and G'' are not described by the standard linear viscoelastic expression in terms of the relaxation modulus.

In this framework, the storage and loss moduli extracted from LAOS experiments should no longer be interpreted as material functions, but rather as effective descriptors of the elastic and dissipative contributions to the response dependent on the strain amplitude.

Despite the strain-dependent storage and loss moduli provide a convenient and widely used description of nonlinear viscoelastic behaviour, they do not capture the full complexity of the stress response once waveform distortions occur. In order to quantify the degree and nature of this distortion, it is necessary to analyze the higher harmonic content of the stress signal. This motivates the use of approaches based on Fourier Transforms, which explicitly account for the non-sinusoidal character of the response under large amplitude oscillatory shear.

1.6. Fourier transform analysis

The responses of materials to SAOS (in which G′ and G″ are strain-independent) tests, $\tau = \gamma_0[G'(\omega)\sin(\omega t) + G''(\omega)\cos(\omega t)]$, contain contributions that are in phase and out of phase with the oscillating deformation, from which the storage modulus G′ and loss modulus G″ can be determined. In the case of LAOS, the shear stress (τ) can be described as in-phase and out-of-phase components of time-domain Fourier series of odd harmonics:

$$\tau = \gamma_0 \sum_{n=1,odd}^{N} [G'_n(\omega,\gamma_0)\sin(n\omega t) + G''_n(\omega,\gamma_0)\cos(n\omega t)] \qquad 1.8$$

In Eq. 1.8, G'_n and G''_n are the amplitudes of the nth harmonics with frequencies $n\omega$. In this representation, only odd harmonics are included as the stress response is assumed to be of odd symmetry for directionality of shear strain or shear-rate, since even harmonics may indicate the occurrence of flow heterogeneities such as secondary flow or wall slip [36] [37]. Up to the limit of the linear viscoelastic regime, the output stress waveform consists only of the first harmonic coefficients, i.e., $n = 1$. In this condition, the material response can be fully characterized by the first order dynamic moduli ($G' \equiv \lim_{\gamma_0 \to 0} G'_1 \; and \; G'' \equiv \lim_{\gamma_0 \to 0} G''_1$). Exceeding the limit of linearity, the first harmonics are not the only signals present due to the distortion of the stress waveform.

The first attempt to take the higher harmonics into consideration for quantitative interpretation of LAOS data was done by comparing the relative intensity of different higher harmonics, dubbed 'overtones' in a musical analogy [38]. In this regard, the intensity of each harmonic can be calculated by:

$$I_n = \sqrt{I'^2_n + I''^2_n} \tag{1.9}$$

In which $I'_n = \gamma_0 G'_n$ and $I''_n = \gamma_0 G''_n$. $I_1, I_3, I_5, \ldots$ in eq. 1.9 are the intensities of the fundamental applied angular frequency (and corresponding response) and its higher odd harmonics of the response. Although FT-rheology is developed based on a robust mathematical framework, there are no clear physical interpretations of what the higher-order harmonics represent, and therefore how to interpret the nonlinear behaviour [39].

1.7. Decomposition through Chebyshev functions

Even if the Fourier decomposition is effective in describing the nonlinear response as a set of harmonics of the in phase and in quadrature response, they lack clear physical meaning. For this reason Ewoldt et al. [39] proposed novel measures, based on the stress decomposition (SD) method introduced by Cho et al. [40], to give meaning to LAOS results. The SD method essentially consists in decomposing the nonlinear shear stress response (τ) into an elastic (τ') and a viscous (τ") stress component as defined in eq. 1.10:

$$\begin{cases} \tau'(t) \equiv \dfrac{\tau(\gamma, \dot{\gamma}) - \tau(-\gamma, \dot{\gamma})}{2} \\ \tau''(t) \equiv \dfrac{\tau(\gamma, \dot{\gamma}) - \tau(\gamma, -\dot{\gamma})}{2} \end{cases} \tag{1.10}$$

Afterward Ewoldt et al. [39] proposed a comprehensive framework for physically interpreting the distorted stress-wave based on a polynomial regression fit. Based on their evaluations, the set of Chebyshev polynomials of the first kind, T_n, is best for this purpose:

$$\begin{cases} \tau'(x:\ \omega,\gamma_0) = \gamma_0 \sum e_n\,(\omega,\gamma_0) T_n(x) \\ \tau''(x:\ \omega,\gamma_0) = \dot{\gamma}_0 \sum v_n\,(\omega,\gamma_0) T_n(y) \end{cases} \quad 1.11$$

Where, x=$\frac{\gamma}{\gamma_0}$ and y=$\frac{\dot{\gamma}}{\dot{\gamma}_0}$ in eq. 1.11 depict the normalized shear strain and shear strain rate while the coefficients "e" and "v" are intended to represent elastic and viscous contributions. The physical interpretation is based on the sign of "e_3" and "v_3" as they determine the concavity of τ' and τ''. According to these coefficients, the following intra-cycle nonlinear interpretations were proposed: strain-stiffening ($e_3 > 0$), strain-softening ($e_3 < 0$), shear-thickening ($v_3 > 0$) and shear-thinning ($v_3 < 0$). Moreover, the nth-order Chebyshev coefficient and Fourier coefficients can be related to each other with eq. 1.12:

$$\begin{cases} e_n = G'_n\,(-1)^{(n-1)/2} \\ v_n = \dfrac{G''_n}{\omega} = \eta'_n \end{cases} \quad 1.12$$

As mentioned earlier, in the nonlinear regime, G′ and G″ are not enough to describe the material response. Using their coefficients Ewoldt et al. also defined new local viscoelastic moduli called the minimum-strain modulus G'_M and large-strain modulus G'_L in eq. 1.13, and the minimum-rate dynamic viscosity η'_M and large-rate dynamic viscosity η'_L in eq. 1.14 [39] [41]:

$$\begin{cases} G'_M = \dfrac{d\sigma}{d\gamma}_{\gamma=0} = \sum nG'_n = e_1 - 3e_3 + 5e_5 - 7e_7 + \cdots \\ G'_L = \dfrac{\sigma}{\gamma}_{\gamma=\pm\gamma_0} = \sum G'_n(-1)^{\frac{(n-1)}{2}} = e_1 + e_3 + e_5 + e_7 + \cdots \end{cases} \quad 1.13$$

$$\begin{cases} \eta'_M = \dfrac{d\sigma}{d\dot{\gamma}}_{\dot{\gamma}=0} = \dfrac{1}{\omega}\sum nG''_n(-1)^{\frac{(n-1)}{2}} = v_1 - 3v_3 + 5v_5 - 7v_7 + \cdots \\ \eta'_L = \dfrac{\sigma}{\dot{\gamma}}_{\dot{\gamma}=\pm\dot{\gamma}_0} = \dfrac{1}{\omega}\sum G''_n = v_1 + v_3 + v_5 + v_7 + \cdots \end{cases} \quad 1.14$$

These local measures were then combined to develop dimensionless indices (eq. 1.15) intended to quantify a relative amount of strain stiffening (S) and shear-thickening (T) respectively:

$$\begin{cases} S = \dfrac{G'_L - G'_M}{G'_L} \\ T = \dfrac{\eta'_L - \eta'_M}{\eta'_L} \end{cases} \quad 1.15$$

S equal to zero corresponds to a linear elastic behaviour, while a positive S indicates intra-cycle strain stiffening behaviour and a negative S indicates intra-cycle strain softening. A shear-thickening ratio equal to zero corresponds to a linear viscous

behaviour, while a positive T indicates intra-cycle shear thickening and a negative T corresponds to intra-cycle shear thinning.

1.8. Payne effect

The Payne effect is one of the most characteristic manifestations of nonlinear viscoelastic behaviour in filled elastomers. It consists in the decrease of the storage modulus *G′* and to the corresponding peak in the loss modulus *G′′*, illustrated in Figure 1.6 observed when the material is subjected to oscillatory deformation of increasing amplitude. This characteristic behaviour represents one of the most important aspects of the viscoelastic properties of filled rubbers, since these materials are often subjected to dynamic stresses and strains in their various applications, directly correlated to this phenomenon.

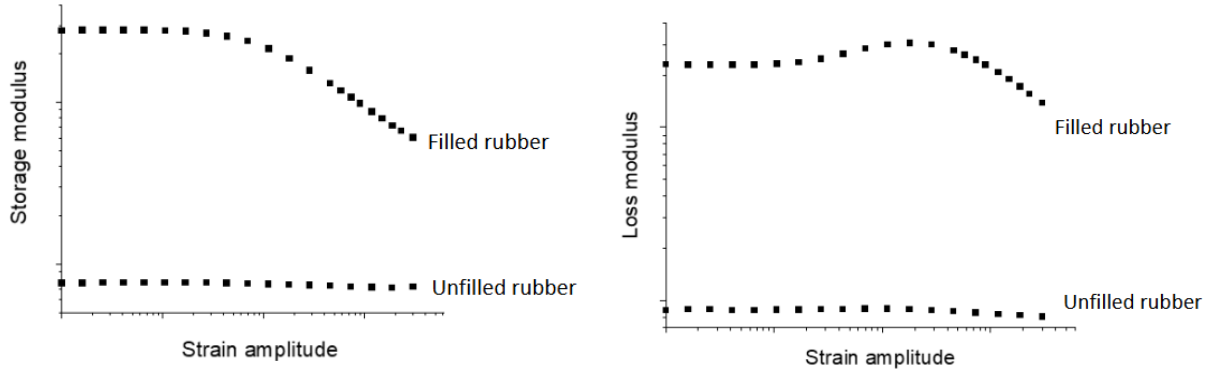

Figure 1.6. Dependence of the storage (on the left) and loss modulus (on the right) on strain amplitude for filled and unfilled rubber [42]

It was first reported by Payne (1962) [42] who observed a strong dependence of *G′* on the strain amplitude after testing a natural rubber filled with carbon black, and attributed it to the breakdown of weak physical linkages between filler particles. Following Payne's pioneering work, several researchers extended his interpretation to other fillers and matrices, highlighting the complexity and confirming the universality of the effect in particulate-reinforced elastomers. Moreover, the introduction of silica as an alternative to carbon black made the phenomenon even more pronounced, because polar silanol groups promote strong filler-filler hydrogen bonding, giving rise to extensive clustering that is easily disrupted under deformation [10].

The Payne effect's origin has been ascribed to the dispersion of filler [43] [44] [45] [46], collapse of filler network [47] [48] [49] or polymer-filler network [50] [51] [52], desorption of rubber chains from the surface of the filler nanoparticles [53] [54], and formation of glass layer surrounding the filler (nano)particles [54] [55] [56]. Despite the variety of microscopic interpretations proposed in the literature, a common and

unifying picture can be drawn. At small strain amplitudes, filler particles or aggregates form a weak, three dimensional network through physical interactions such as van der Waals forces or hydrogen bonding, which contributes to stiffen the material. As the deformation amplitude increases, this network progressively breaks down, leading to a reduction of the storage modulus and to enhanced energy dissipation. Once the filler network is largely disrupted, the mechanical response becomes increasingly governed by the polymer matrix, by local filler-rubber interactions, and, when present, by the chemical crosslink network.

Nowadays the Payne effect is not only an observed and studied phenomenon, but a diagnostic tool for assessing filler dispersion quality, interfacial coupling efficiency, curing performance and mixing homogeneity.

1.9. Leblanc-Nijman model

One of the most physically grounded approaches to analyze LAOS test results and for quantifying the nonlinear viscoelastic behaviour of filled polymer systems is the Leblanc-Nijman model [57], which consists of analyzing the evolution of harmonic content in the torque during oscillatory tests.

When a sinusoidal strain is applied to a filled rubber, the resulting stress response deviates from a perfect sine wave producing higher odd harmonics that gives information about the degree of nonlinearity. Leblanc and Nijman proposed that the relative harmonics content, I_3/I_1 ; I_5/I_1 ; ..., can be expressed as a function of strain amplitude γ in eq. 1.16:

$$TH(\gamma_0) = (TH_m + \alpha\gamma_0) \times \{[1 - \exp(-\alpha\gamma_0)]^{TH_m} + B(C\gamma_0)^{D-1}\exp[-(C\gamma_0)^D]\} \quad 1.16$$

In practice it is most often applied for the so-called total torque harmonic content TTHC: $(I_3 + I_5 + I_7 + I_9)/I_1$, although it accounts for the sum of all higher odd harmonics, the shape of the TTHC curve is mainly controlled by the evolution of I_3/I_1, since the third harmonic is the dominant nonlinear contribution in this case. The physical meaning of the five parameters in this empirical expression is easily understood when one considers that it consists of three members, as illustrated in Figure 1.7.

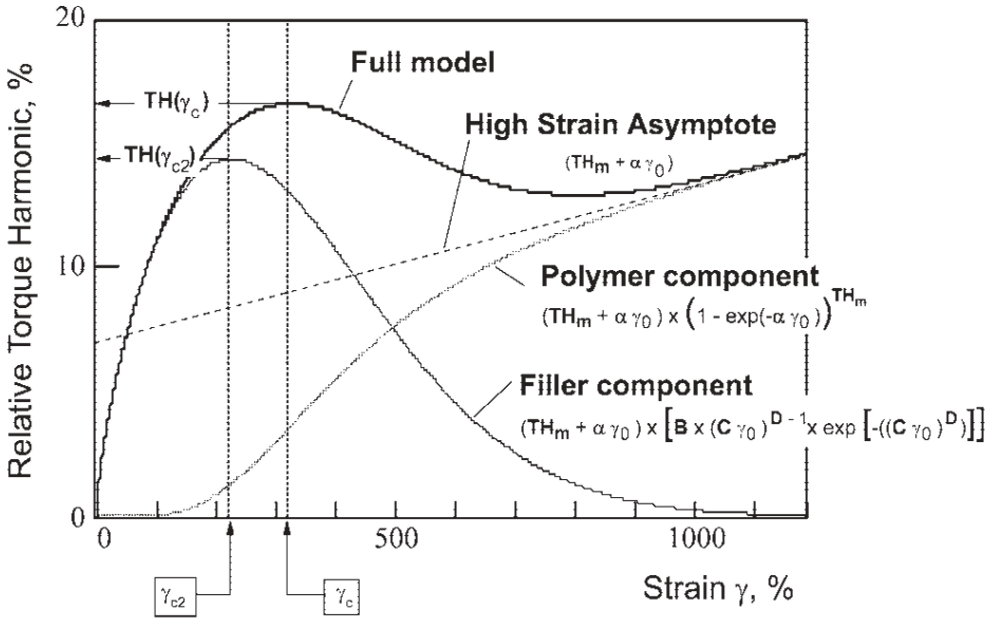

Figure 1.7. Modeling the relative torque harmonics variation with strain amplitude of filled materials [57]

The first term, $TH_m + \alpha\gamma_0$, describes the asymptotic high strain behavior.

The polymer component, $(TH_m + \alpha\gamma_0) \times [1 - \exp(-\alpha\gamma_0)]^{TH_m}$, describes the polymer response, and is consistent to the unfilled rubber behavior.

The filler component, $(TH_m + \alpha\gamma_0) \times \{B(C\gamma_0)^{D-1}\exp[-(C\gamma_0)^D]\}$, describes the filler response.

As can be seen, at low strain, the nonlinear character is essentially controlled by the filler component, while at higher strain, the influence of the filler vanishes and harmonics variation is essentially controlled by the polymer component. The maximum of the filler component curve corresponds to a critical strain, i.e., γ_{c_2}, at which decreasing polymer-filler interaction would start to override the nonlinearity enhancement due to the dispersed phase.

Besides giving a picture which is correlated with Payne effect physics, the model is able to fit both the behaviour of both uncured and cured filled elastomers. In uncured systems, the nonlinearity primarily originates from the breakdown and reformation of the filler-filler network, while in cured materials additional contributions arise from the chemical crosslink network, whose elasticity modifies the strain dependence of the harmonic response. The model parameters thus provide insight into how curing, silanization, or filler surface modification alter the interplay between physical and chemical reinforcement.

Overall, the LeBlanc-Nijman model provides a bridge between the harmonic description of LAOS and the microstructural interpretation of filled rubber behavior,

allowing the complex nonlinearity of elastomeric systems to be summarized through a small number of physically interpretable parameters.

2 Materials and Methods

2.1. Materials

The experimental work involved testing different materials comprising SLR4630 (styrene-butadiene rubber), a standard grade of SBR used in the tire industry for the manufacture of winter and all season applications, each reinforced with 75 phr (parts per hundred rubber - grams of a particular component per 100 grams of rubber matrix), of silica Zeosil 1165 MP.

While silica increases stiffness and abrasion resistance, its surface silanol groups make it polar and prone to hydrogen-bonding aggregation, leading to poor compatibility with the non-polar SBR phase and to the formation of filler clusters.

To improve the rubber-filler interaction, different concentrations of bis[3-(triethoxysilyl)propyl] tetrasulfide (TESPT) were added. As a result, increasing the TESPT content promotes finer filler dispersion and also, introducing sulfur during the curing process, influences the final chemical network. Because of this sulfur addition, the amount of elemental sulfur was corrected in selected formulations so as to compare materials with similar cured network density but different silane concentrations. In total, five uncured formulations were prepared, varying the TESPT and the sulfur content, as reported in table 2.1 along with the illustration of the nomenclature that will be adopted from this point throughout the thesis.

Table 2.1. Labels used in the present work based on the concentration of TESPT, low (L), medium (L), high (H) and on the eventual correction of the sulfur content, increased for compound L (L_c) and decreased for compound H (H_c).

Species [phr]	**L**	**M**	**H**	$\mathbf{L_c}$	$\boldsymbol{H_c}$
Silica	75	75	75	75	75
TESPT	3.75	6	8.25	3.75	8.25
Sulfur	1	1	1	1.27	0.73

In addition to the silica filler and the coupling agent various species with fixed concentrations were incorporated during the rubber compounding process, each serving a unique purpose. They are detailed in table 2.2. The antioxidant 6PPD, or N-(1,3-dimethylbutyl)-N'-phenyl-p phenylenediamine, and TMQ (polymerized 2,2,4-trimethyl-1,2-dihydroquinoline) were included to protect the rubber from oxidative degradation. CBS, known chemically as N-cyclohexyl-2-benzothiazole sulfenamide, functioned as an accelerator to advance the vulcanization process. Zinc oxide (ZnO) served as an activator, facilitating the overall vulcanization reaction and ensuring a uniform cure throughout the compound. Lastly stearic acid acts as a vulcanization activator and it also reacts with zinc oxide to form zinc stearate that can act as a release agent and processing aid.

Table 2.2. Other species concentrations, common to all compounds

Species	**Concentration [phr]**
Stearic Acid	2
6PPD	3
TMQ	1.5
Zno	1.5
CBS	3

The materials were kindly supplied by Pirelli&C S.p.A, who also carried out the mixing operation. The calendered sheets received were stored at low temperature (4°C) in a refrigerator, and warmed at room temperature for 30 min before being tested.

2.2. Dynamic Mechanical Tests

In this particular section, we provide a comprehensive and detailed description of the measuring instrument and the various test protocols that have been utilized in our procedures.

2.2.1. Testing apparatus

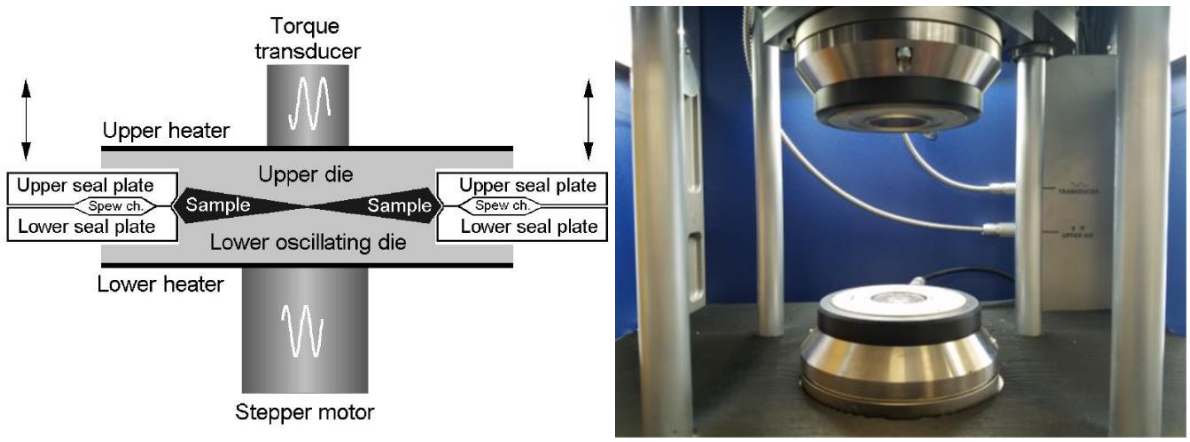

Figure 2.1: Scheme of the testing apparatus (on the left) and picture of the Premier RPA (on the right

Most of the experiments were carried out using the Rubber Process Analyzer (Premier RPA) from Alpha Technologies showed in Figure 2.1, a closed chamber dynamic mechanical rheometer specifically designed for the characterization of rubber compounds in both uncured and vulcanized states.

The instrument operates with a sealed biconical die system, in which a small amount of material (about 6g) is confined by two opposing dies. During testing, the lower die oscillates in torsion through a self-controlled electric motor that imposes the strain amplitude and oscillation frequency while the upper die is fixed and connected to a torque transducer that measures the material response. The system software then converts the torque signal into fundamental viscoelastic parameters such as the storage modulus (G′), loss modulus (G″), and loss tangent (tan δ).

A pneumatic pressure system ensures that the die cavity remains sealed during the measurement, preventing at the same time slippage at the die-sample interface, thus improving reproducibility even when the material undergoes large deformations or dimensional changes during vulcanization.

Thanks to heating elements and thermocouples embedded directly inside the dies, the Premier RPA can accurately control the cavity temperature over a wide range (ambient to ≈ 230 °C) during both isothermal and temperature sweep tests.

A smaller portion of the tests was carried out using a RPA sub-Zero (Alpha Technologies), which operates in the same manner as the previously described rheometer, with two main differences: it allows a wider temperature range (approximately -25°C to 230 °C), and provides the possibility of applying additional chamber pressure compared to the previous case. The latter is the feature exploited in this work.

2.2.2. Sinusoidal Oscillatory Test in simple condition

To investigate the viscoelastic response of the materials, the experimental procedure relied on the application of various histories of oscillatory shear deformations with sinusoidal waveforms. By varying the amplitude of the strain it was possible to capture the different aspects of the material's behaviour, from the linear regime to the strongly nonlinear domain. The experimental parameters considered are outlined in Eq. 2.1 where γ_0 is the amplitude of the shear strain and ω is the frequency.

$$\gamma(t) = \gamma_0 \sin(\omega t) \qquad 2.1$$

2.2.3. Large Amplitude Oscillatory Shear (LAOS) Test

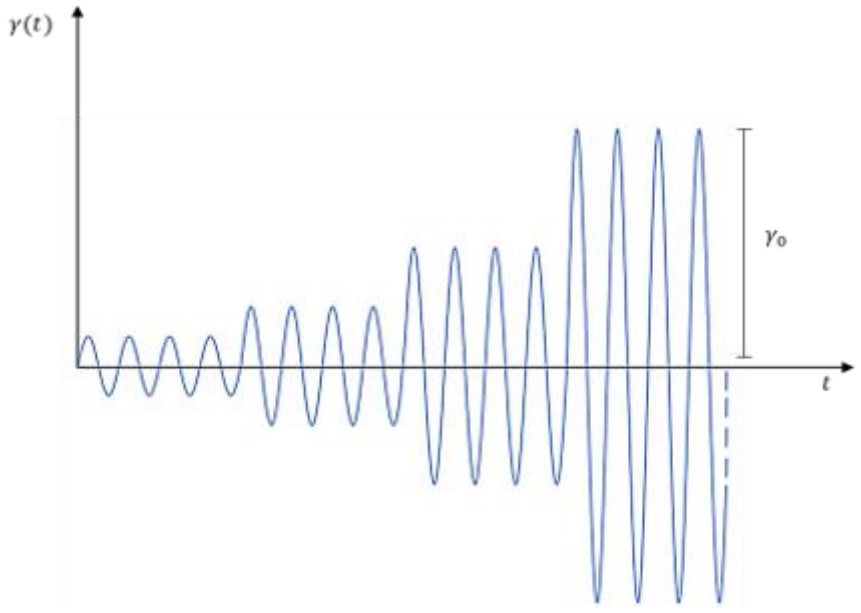

Figure 2.2. Scheme of an oscillatory applied strain test with increasing strain amplitude γ_0

The most utilized test for investigating the Payne effect involves deforming the specimen with progressively increasing shear strain amplitudes, γ_0, at constant angular frequency, ω, as sketched in Figure 2.2. The shear strain increase occurs by steps. This method typically focuses on the material's steady-state behavior, therefore

the data acquisition at each step has to start until the steady state is reached. The specific parameters utilized in these tests of the present work are reported in the table that follows:

Table 2.3. Control parameters of the increasing strain amplitude test

	γ_0 [%]	γ_0 [%]	Frequency [Hz]	Temperature [°C]
Uncured test	0.1	1000	0.5	50
Cured test	0.1	200	0.5	50

As shown in Table 2.3, the maximum strain applied in the tests for cured samples was lower than that used for uncured ones. This choice was made because, beyond approximately 200% strain, part of the cured specimens exhibited visible damage, making the measurement unreliable. The frequency was selected so that the RPA could maintain it also at the highest shear strain amplitudes (≈1000%). The testing temperature was set to the lowest value recommended by the instrument manufacturer, 50°C, ensuring stable control and avoiding any unintended curing during the measurements.

2.2.4. Constant strain amplitude test

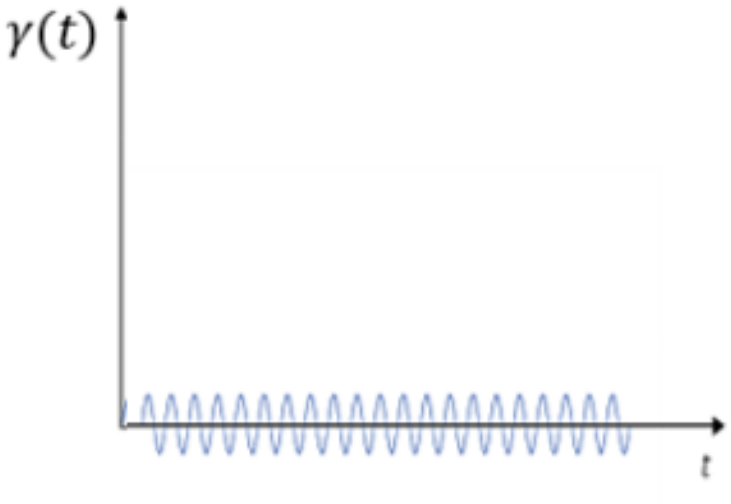

Figure 2.3. Scheme of a constant strain amplitude test

To monitor the temporal variation in dynamic response, it is possible to perform a test at a constant shear strain amplitude and frequency. In this work the test has been used to evaluate the evolution of the curing kinetic and the crosslinking degree in isothermal condition. The selected test parameters are: $\gamma_0 = 0.1\%$; $\omega = 0.5\text{Hz}$. In this way the test is performed in the linear regime, and it doesn't interfere with the curing process.

2.2.5. Curing test

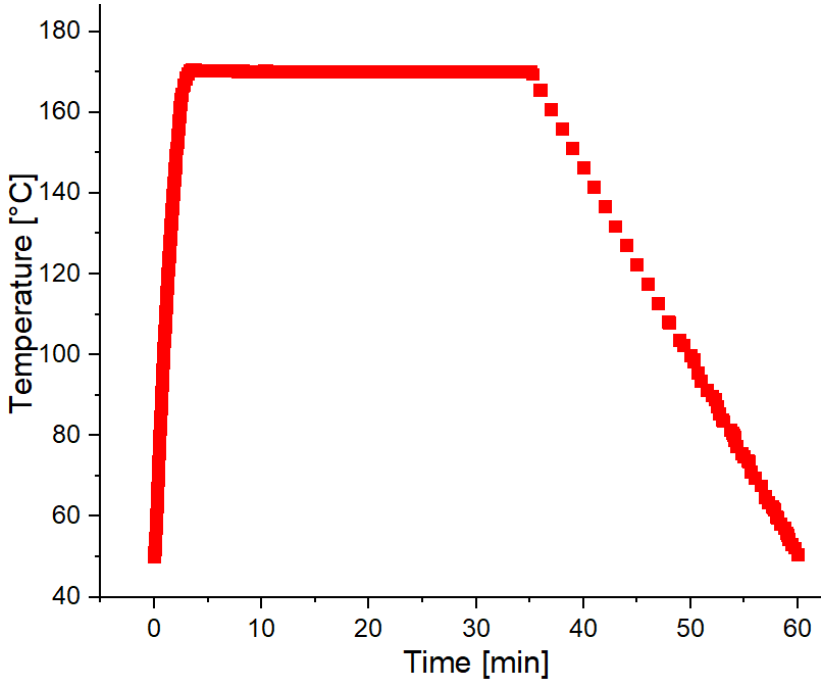

Figure 2.4. Scheme of the thermal history applied for curing

The curing sequence was carried out in accordance with international standards for rotorless cure-meters (ASTM D5289), which require the specimen to be brought from the initial temperature (T_0) to the curing temperature as rapidly as possible. In this work, the curing temperature was set to 170 °C, as recommended by Pirelli. The Premier RPA was programmed to reach this setpoint within a maximum of 5 minutes; in practice, the heating ramp was completed in approximately 3 minutes, after which the remaining 2 minutes were maintained under isothermal conditions. The test then continued for a further 30 minutes at 170 °C, a time longer than the recommended by the producer to ensure that the vulcanization process was essentially complete. Finally, a controlled cooling stage from 170 °C down to 50 °C in 25 minutes, using a linear ramp was carried out. The slow cooling rate was deliberately selected, since faster ramps occasionally produced anomalous variations in G′, most likely caused by thermal shock and internal stresses, which could lead to artifacts in the measurement.

2.2.6. Effect of different cooling ramps

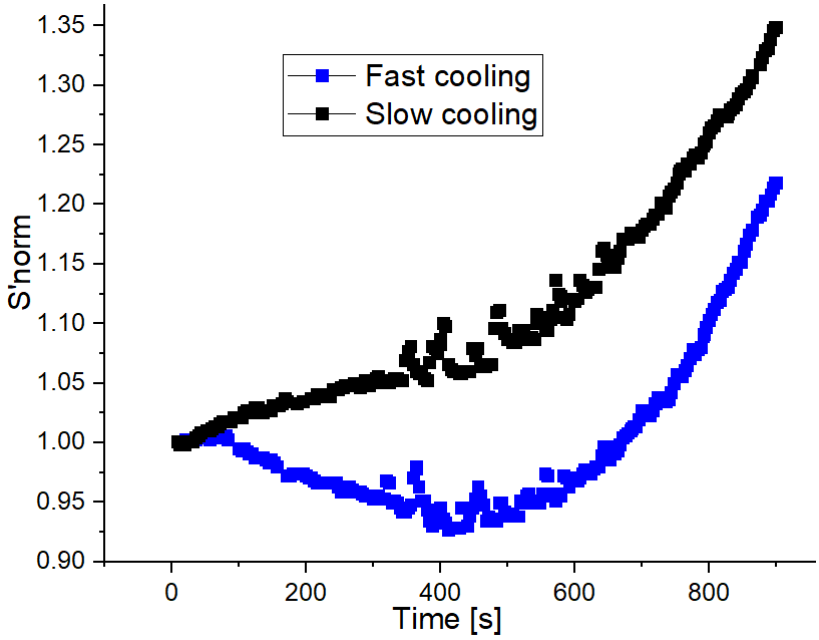

Figure 2.5. Evolution of the storage torque S′ during post-cure cooling under different cooling rate

During post-cure cooling under linear oscillatory conditions, the expected trend is a monotonic increase of S′(t) as temperature decreases. With a fast cooling ramp, however, an initial drop in S′ is occasionally observed as shown in Figure 2.5, followed by only partial recovery, resulting in a lower final value than that obtained with slow cooling. The most consistent interpretation is that rapid cooling generates bigger thermal gradients between the die walls and the specimen core, causing differential contraction that can leave internal stresses that do not fully relax, lowering the final S′ value.

2.2.7. Effect of wrong sample positioning

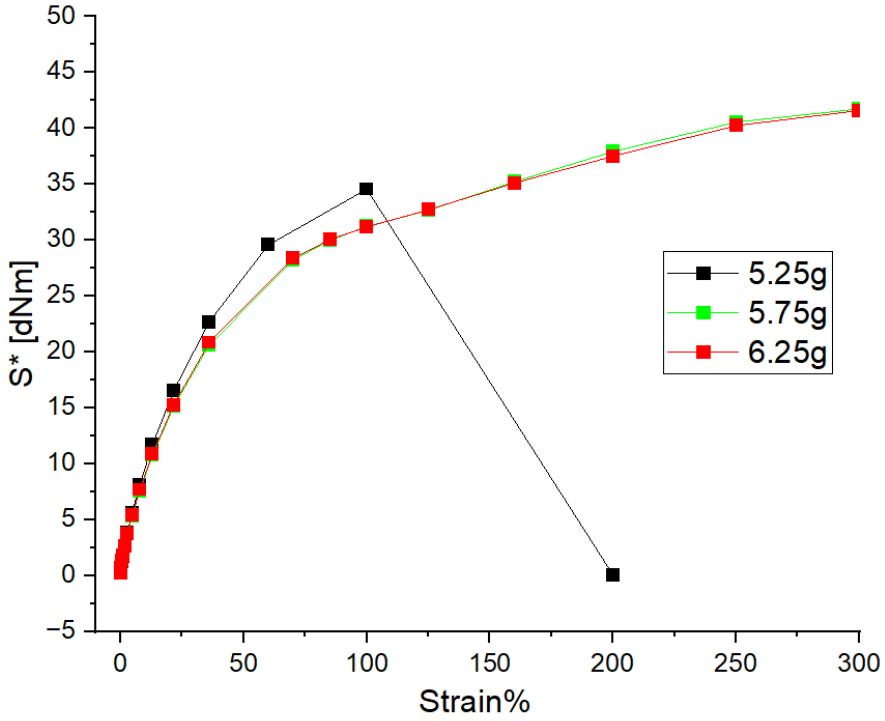

Figure 2.6. Evolution of the torque signal with the strain amplitude for one sample of 5.25g (black), one of 5.75g (green), and one of 6.25g (red)

All the tests were conducted using a sealed biconical die geometry, designed to provide uniform shear and to minimize wall slip, provided that the cavity is completely filled and properly clamped under the prescribed normal pressure.

In this configuration, loading a slightly excessive amount of material is harmless, as any surplus compound is simply expelled as flash during die closure, while the correct gap and contact conditions are maintained. By contrast, insufficient filling represents the only critical preparation error. If too little material is loaded, the cavity is not fully occupied and the normal pressure is not transmitted uniformly. Small voids or unconfined regions may remain, reducing the effective contact area and allowing partial detachment or slip at the die surfaces. At large strain amplitudes this loss of confinement gets worse leading to the drop toward the instrument's noise of the torque signal as shown in Figure 2.6, invalidating the high strain data. This drop of the torque signal occurred occasionally also for tests performed with specimen mass of 5.5g. To avoid this instability, a minimum mass of 5.75 g has been adopted for all subsequent experiments, for which no signal collapse was observed.

3 Experimental Results

In this chapter attention is directed towards the curing kinetics and the nonlinear response exhibited by filled rubbers when subjected to increasing strain amplitude, known as the Payne effect. Specifically, the results are intended to demonstrate how variations in TESPT content and sulfur concentration influence the development of the crosslink network, the evolution of filler-filler and filler-rubber interactions, and consequently the strain-dependent behaviour of both uncured and cured compounds.

3.1. Curing kinetics

Dynamic mechanical analysis, particularly through constant strain amplitude tests performed under isothermal conditions, represents a well-established method for monitoring the curing kinetics of rubber compounds. By tracking the evolution of torque as a function of time, it is possible to follow the progressive development of the crosslink network.

In this work, the curing behavior of the investigated compounds is analyzed in terms of the conventional rheometric parameters. Table 3.1 reports the characteristic curing times t_{10} and t_{90}, together with the interval $\Delta(t_{90}\text{-}t_{10})$, which provides an estimate of the effective crosslinking rate. Figure 3.1 illustrates the time evolution of the normalized torque S'/S'_{final}, where S' represents the measured torque and S'_{final} the plateau value reached at the end of curing.

The analysis of these parameters allows a direct comparison of the influence of TESPT content and sulfur concentration on the rate of network formation and on the final extent of crosslinking, providing the structural framework necessary for the subsequent interpretation of the nonlinear viscoelastic response.

Table 3.1. Characteristic curing time to reach 10% and 90% of the total torque increase together with the effective cure interval ($t_{90} - t_{10}$)

Compound	t10% [sec]	t90% [sec]	Δt [sec]
L	62.04	1060.60	998.56
M	68.17	1024.07	955.90
H	54.27	761.23	706.96
Lc	50.67	1053.27	1002.60
Hc	44.97	788.60	743.63

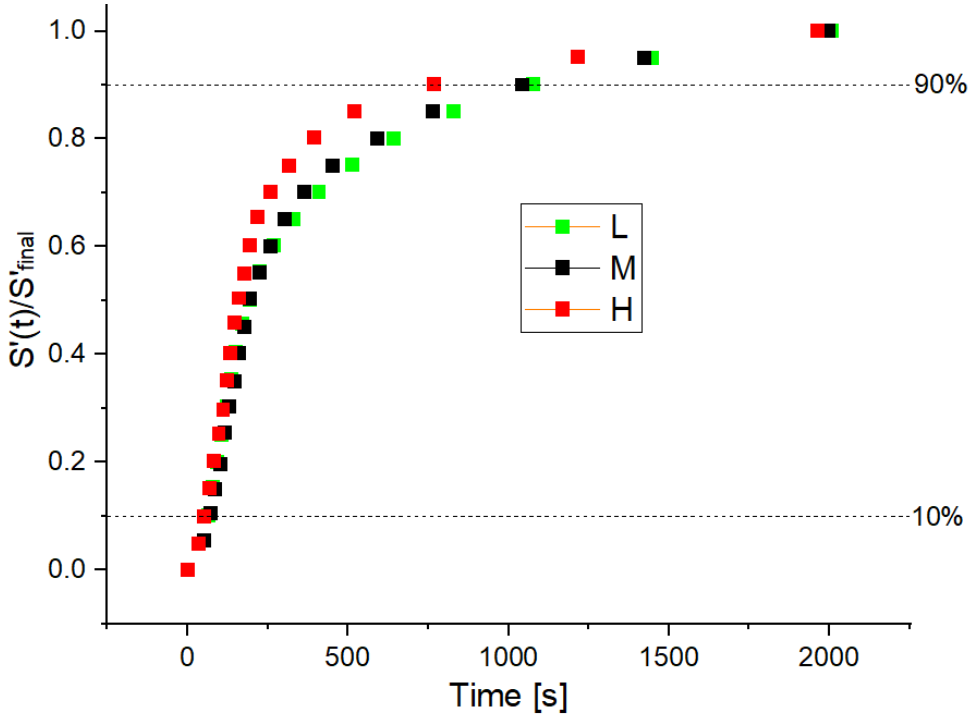

Figure 3.1. Evolution of the storage torque S' during vulcanization normalized to its final value

Figure 3.1 and Table 3.1 show that the curing kinetics follow the expected order H > M > L, indicating a faster cure for the higher-TESPT formulation.

This trend is consistent with the dual role of TESPT as both sulfur donor and coupling agent: by supplying additional sulfur, it promotes network formation, while its improved rubber-silica coupling and enhanced filler dispersion increase the availability of reactive sites near the filler surface and reduce the adsorption of curatives on the silica surface, enhancing the efficiency of the curing system. Interestingly, compound M appears closer to L than to H in terms of curing kinetics, suggesting a non-linear dependence on the TESPT content.

Comparing compounds with identical TESPT content but different sulfur levels (L-Lc and H-Hc) shows that the modest sulfur increase does not induce a systematic variation of Δt. Only slight variations in t_{90} are observed, and even these are limited, confirming that TESPT concentration, rather than the small sulfur adjustment, is the principal factor governing the curing kinetics.

3.2. Payne effect in uncured compounds

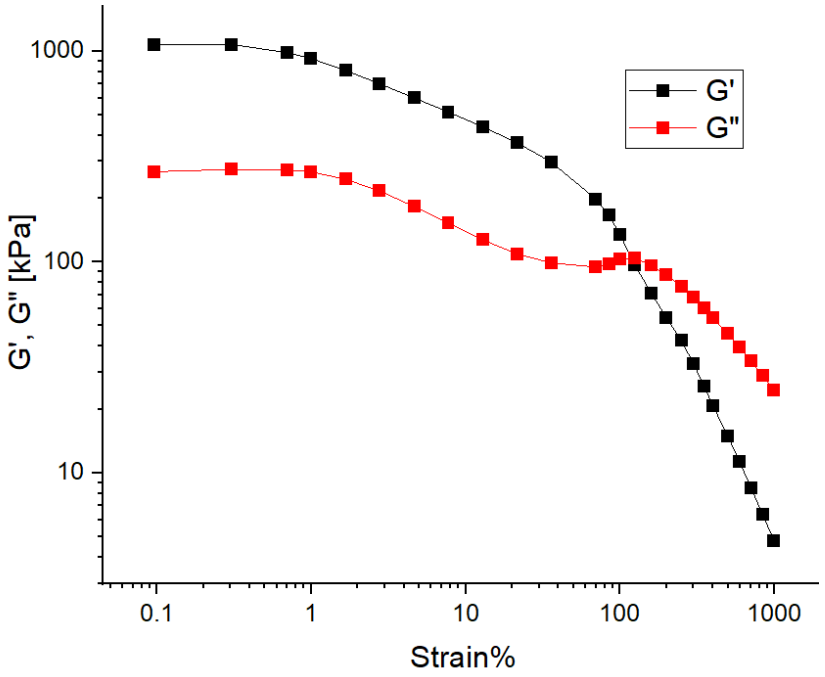

Figure 3.2. Storage (G′) and loss (G″) modulus in test performed pre-cure at $\omega = 0.5Hz$ and $T = 50°C$ for compound M

Figure 3.2 illustrates the nonlinear dependence of the dynamic moduli on strain amplitude, plotted on a double logarithmic scale for the uncured compounds.

At small strain amplitudes, an initial plateau defines the linear viscoelastic region, limited to the first two points (0.1% and 0.3%), where both G′ and G″ are independent of strain amplitude. In this range, the applied stress is too small to disturb the microstructure of the compound. Beyond this region, the material enters the nonlinear regime, where the Payne effect becomes evident. Here, G′ decreases monotonically, reflecting the progressive breakdown of the filler-filler network. At the same time, although less pronounced, a small absolute maximum of G″ appears at the onset of the nonlinear regime, associated with additional dissipation due to the breaking and reforming of weak physical bonds. As the strain amplitude further increases, $\tan\delta$ rises and the material gradually transitions toward a liquid-like response. Near the crossover condition ($G' \approx G''$, $\tan\delta \approx 1$), G'' exhibits a second relative maximum at medium-to-high strain amplitudes. Beyond the crossover, where $\tan\delta > 1$ and $G'' > G'$, becomes dominated by the polymer matrix. Subsequently G″ decreases due to the progressive alignment and reduced friction of the matrix. Meanwhile, G′ does not reach a second plateau, as the sample is uncured and lacks a chemical crosslinking network capable of restoring elasticity at large deformations.

3.2.1. Comparison among uncured compounds

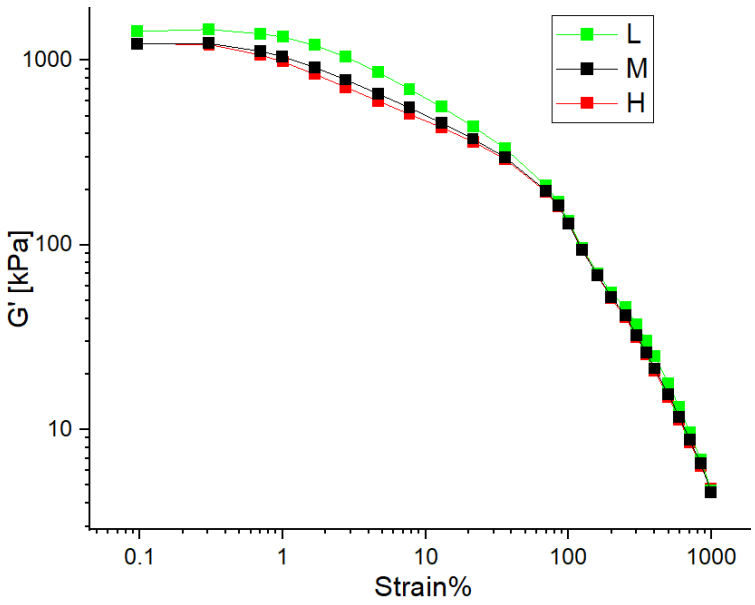

Figure 3.3. Storage modulus G′ pre-cure versus on the strain amplitude showing the dependency on the TESPT content

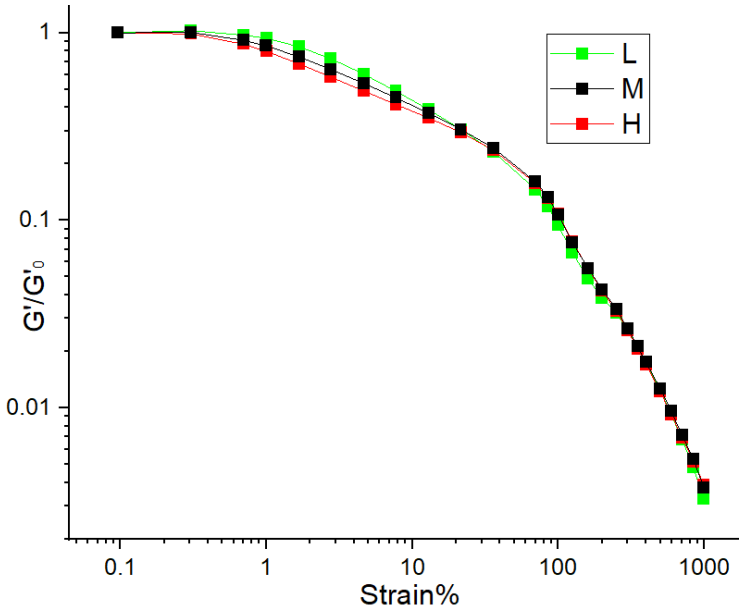

Figure 3.4. Storage modulus G′ pre-cure normalized to its value at $\gamma_0 = 0.1\%$ versus on the strain amplitude showing the dependency on the TESPT content

In the comparison among uncured formulations that differ only in TESPT content (L, M, H), Figure 3.3 shows the storage modulus G′ in the linear viscoelastic regime attains higher values for formulation L than for M and H, consistent with a more pronounced

filler-filler physical network when the rubber-silica coupling is weaker. In the nonlinear regime, G′ decreases with increasing strain amplitude for all formulations (Payne effect), yet remains higher for L up to approximately $\gamma \simeq 85\%$, where the curves converge since the breakdown of the filler-filler network is over. In the intermediate range (200-700%), with $\tan \delta > 1$, small differences between curves persist, always higher values for L, suggesting residual microstructural differences. Any residual difference seems to vanish at higher strain ($\sim 1000\%$) in line with a response dominated by the matrix, which is identical for all compounds. Analyzing G'/G'_0 in Figure 3.4 it can be seen that the initial decrease after the onset of nonlinearity is steeper for higher-TESPT compounds.

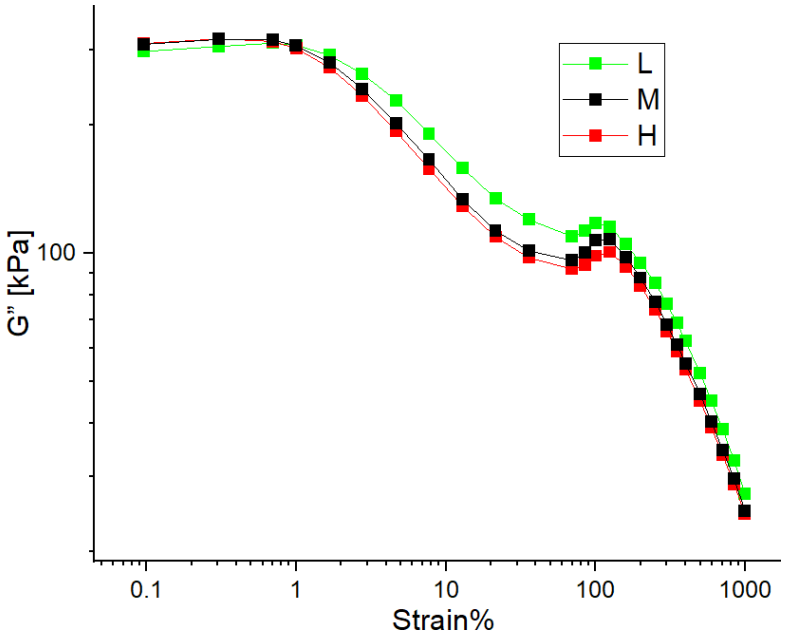

Figure 3.5. Loss modulus G″ pre-cure versus on the strain amplitude showing the dependency on the TESPT content

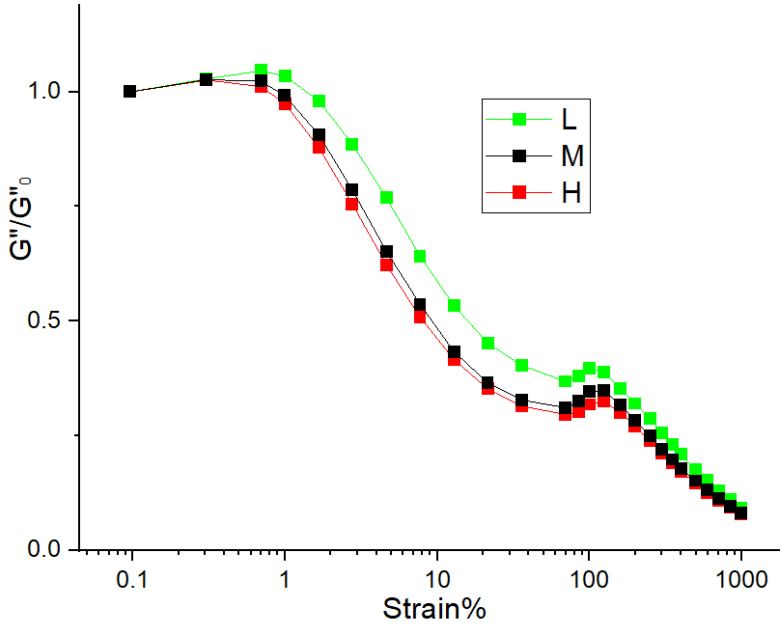

Figure 3.6. Loss modulus G″ pre-cure normalized to its value at $\gamma_0 = 0.1\%$ versus on the strain amplitude showing the dependency on the TESPT content

The evolution of G″, illustrated in Figure 3.5 and Figure 3.6, supports this interpretation. At low strains, just beyond the linear region, the first (barely observable) local maximum of G″ is more pronounced and shifted to slightly higher strain in L, consistent with a more heterogeneous structures with larger clusters and a greater number of filler-filler bonds. With further increase in strain, a second local maximum of G'' appears at medium-high deformation, in the proximity of the crossover ($G' \approx G''$), occurring at lower strain for lower-TESPT compounds. Beyond this point, where $\tan\delta > 1$, the differences among formulations tend to diminish, although they persist slightly in the order $L > M > H$.

It is noteworthy that, in contrast with the curing kinetics, the analysis of G′ and G″ of the uncured compounds show compound M closer to H than to L across all the explored strain range.

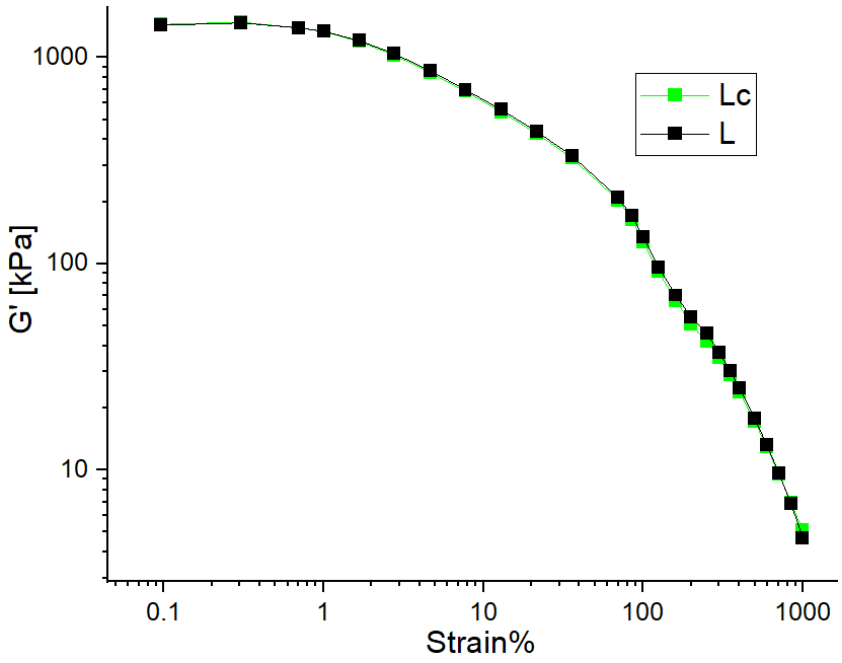

Figure 3.7. Storage modulus G′ pre-cure versus on the strain amplitude showing the dependency on the sulfur content for low-TESPT compounds

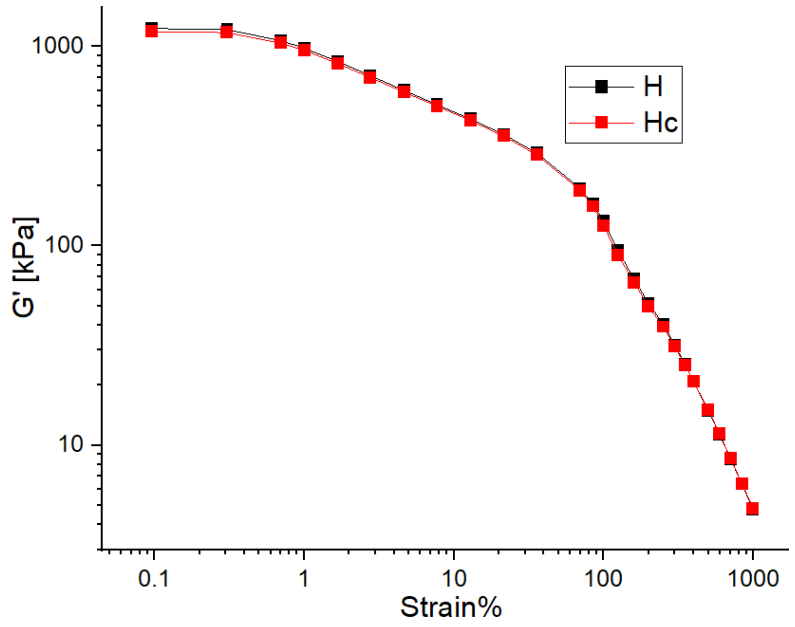

Figure 3.8. Storage modulus G′ pre-cure versus on the strain amplitude showing the dependency on the sulfur content for high-TESPT compounds

In the uncured comparison between the L-Lc and H-Hc pairs, the G′ curves, illustrated in Figure 3.7 and Figure 3.8, are essentially indistinguishable, both in the linear regime and throughout the subsequent softening region. This result is consistent with the fact that, prior to vulcanization, elemental sulfur remains chemically inactive under the

present testing conditions, and such minor variation doesn't alter the pre-cure microstructure of the compounds.

3.2.2. Qualitative analysis of Lissajous curves

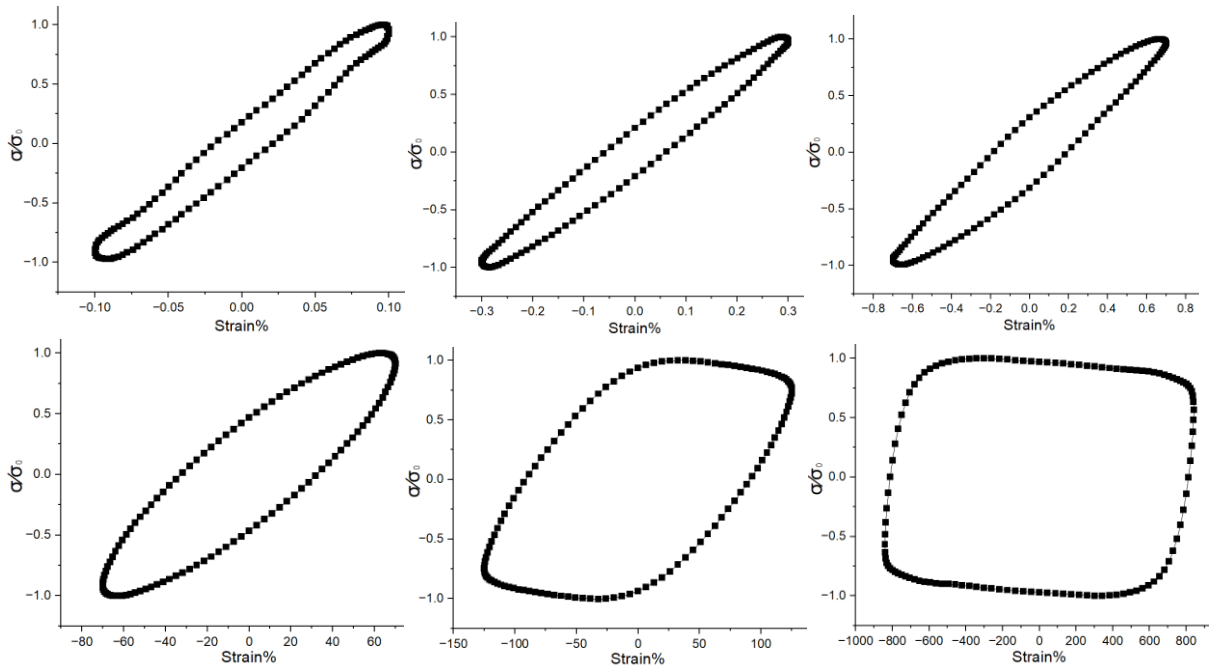

Figure 3.9. Lissajous plots in tests performed pre-cure for compound M at strain amplitudes of 0.1% (a), 0.3% (b), 0.7% (c), 70% (d), 125% (e), 840.9% (f)

A preliminary qualitative analysis of the Lissajous stress-strain plots offers a direct visualization of how the viscoelastic response evolves with strain amplitude, visible in Figure 3.9, complementing the information obtained from the amplitude sweep curves of G' and G".

At very small deformations (γ_0 = 0.1% - figure 3.9a), the torque signal approaches the resolution limit of the instrument, and the resulting ellipse shows visible noise at its extremities. These oscillations, concentrated where the velocity is nearly zero, are attributed to inertial and frictional effects intrinsic to the measuring system rather than to the material itself, and should not be interpreted as a real material non-linearity.

At γ_0 = 0.3% (figure 3.9b), the loop is almost perfectly elliptical, confirming that the response is linear and dominated by a single sinusoidal component; small distortions are still concentrated at its extremities, so still due to the instrument noise.

At $\gamma_0 \approx$ 0.7% (figure 3.9c), the first deviations from linearity appear exhibiting a slight broadening of the ellipse, reflecting the onset of the nonlinear response. The distortion gets more pronounced as the strain increases until $\gamma \approx$7.74%, indicating the progressive

rupture of the filler-filler network. Beyond this point, the distortion decreases, indicating that the physical network of filler clusters has been largely disrupted.

At $\gamma_0 \approx 70\%$ (figure 3.9d), the material displays an almost perfectly elliptical loop once again. In this region, the filler-filler network has been almost entirely disintegrated, while at the same time, the polymer matrix is still in its linear regime: the material therefore exhibits a transiently sinusoidal response. The concurrent minimum of G″ confirms that energy dissipation is at its lowest level, and the Lissajous loop effectively marks the transition between the filler-dominated and the matrix-dominated regime.

Further increasing the strain, particularly after $\gamma_0 \approx 125\%$ (figure 3.9e), where G′ and G″ become comparable and tan δ approaches unity (see figure 3.2), the loops widen again, signaling a strong increase in dissipative phenomena arising from frictional interactions at filler-rubber interfaces and from chain slippage within the stretched polymer network.

Beyond this point, at the highest explored strains, the filler-filler network can be considered entirely disrupted, the loops are almost rectangular consistent with a predominantly viscous response (G″>>G′). The mechanical behaviour, in the absence of a crosslinked network, is therefore governed by the viscoelastic flow of the polymer matrix, characterized by chain slippage and reduced number of entanglements.

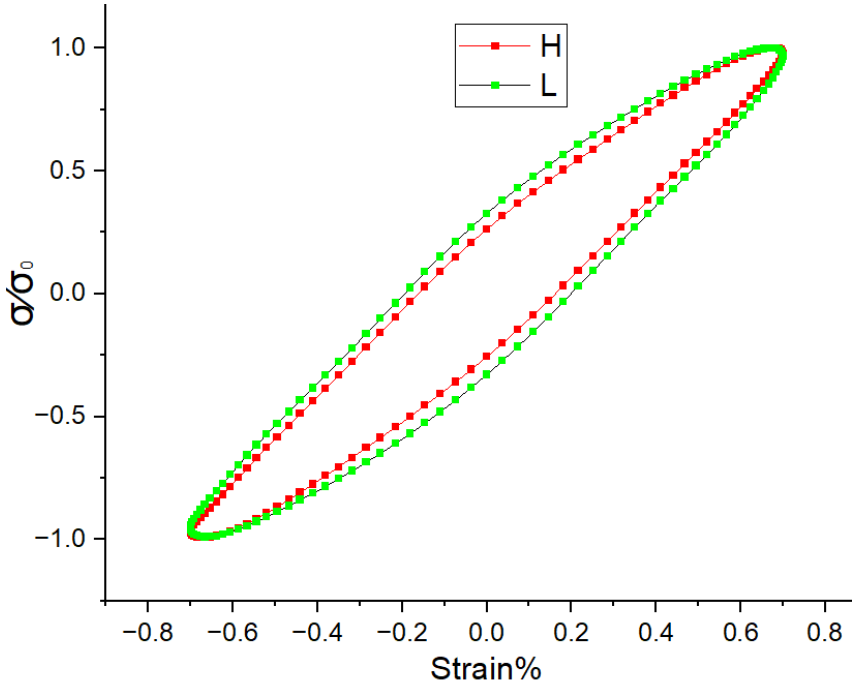

Figure 3.10. Lissajous Plots with strain amplitude 0.7% for visually evaluating enclosed area for compound L and H

No evident differences in the degree of distortion can be identified among the compounds; the Lissajous loops mainly differ in their enclosed area across specific strain ranges visually evaluated like in Figure 3.10. Noticeable distinctions arise only below 70%, within the nonlinear regime. Between 3% and 13% strain, compound H exhibits slightly larger areas than L, indicating a higher number of filler-filler bond breakages in the first part of nonlinear regime. Conversely, from 13% to 35%, the trend reverses, as the larger and more strongly flocculated clusters in L require higher strain amplitudes to be fully disrupted, leading to greater hysteretic losses in this range. The comparison between each compound and its sulfur-adjusted counterpart (L vs Lc and H vs Hc) revealed no appreciable differences in the shape or area of the Lissajous loops across the explored strain range, confirming that, before curing, small variations in elemental sulfur concentration do not influence the viscoelastic response.

3.2.3. Harmonic ratio analysis (I_3/I_1)

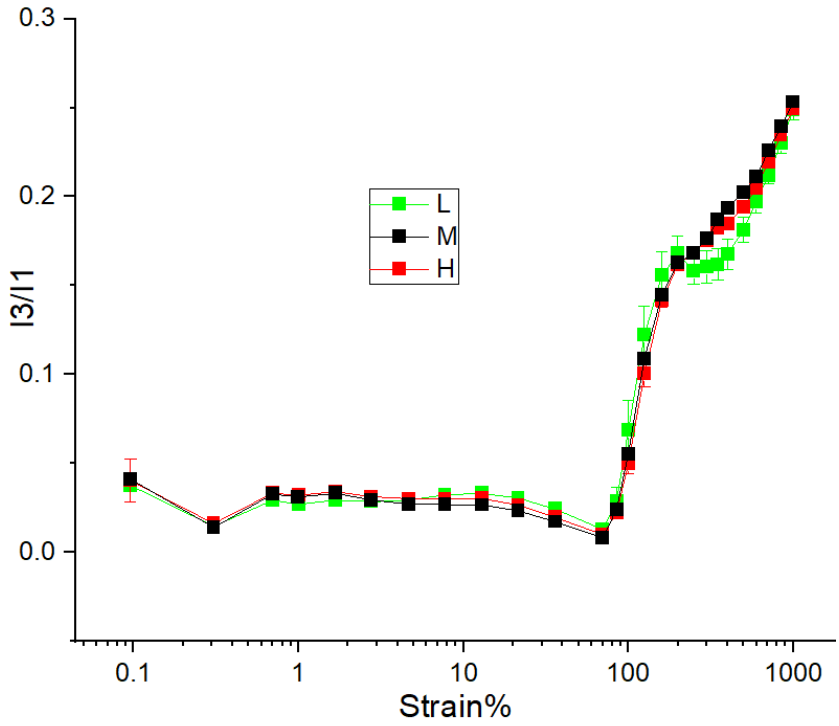

Figure 3.11. Harmonic ratio I_3/I_1 pre-cure versus on the strain amplitude showing the dependency on the TESPT content

Figure 3.11 reports a quantitative evaluation of the nonlinear viscoelastic behaviour that can be obtained from the analysis of the harmonic content of the stress signal, in this case the ratio $I_3/I_1 = S_3^*/S_1^*$ compares the amplitude of the third harmonic to that of the first providing a direct measure of the deviation from sinusoidal behavior and thus of the overall intra-cycle nonlinearity.

At very small amplitudes ($\gamma_0 \approx 0.1\%$), I_3/I_1 displays artificially high values due to instrumental noise, a minimum follows at $\gamma_0 \approx 0.3\%$, corresponding to the purely linear viscoelastic regime, where the stress response is nearly sinusoidal and higher harmonics are absent. As the shear strain amplitude increases beyond the linear regime, I_3/I_1increases around 0.7%. This marks the onset of nonlinearity associated with the initial rupture of weak filler-filler contacts and the first distortions of the Lissajous ellipse. Between 0.7% and approximately 13%, the ratio remains almost constant.

Beyond 13%, I_3/I_1 begins to decrease, indicating that the filler network is progressively exhausted and that the corresponding dissipative mechanisms are diminishing. The ratio reaches an absolute minimum around 70%, which once again identifies the transition zone where the filler network is fully disrupted but the polymer matrix has not yet developed significant nonlinear response. This "neutral" region corresponds to the nearly elliptical Lissajous loops and the minimum of G" commented before.

At higher amplitudes, the behaviour of the compounds acts similarly to what has already been observed for the parameter S: the L compound has a maximum at 200%, then decreases, remains constant until 400% and then increases rapidly again; the stronger interfacial coupling in H instead prevent the decrease in I_3/I_1 sustaining higher values and a smoother transition between the filler dominated and the matrix dominated region.

Small differences can also be detected after the onset of nonlinearity, at smaller strain H has higher values than L, indicating that the weaker filler network begins to distort earlier, while L needs higher strain to completely break its bigger clusters, highlighted by higher values after 7%.

The sulfur-adjusted comparisons (L-Lc and H-Hc) don't show any clear difference between them, in particular the smoother transition after 200% for higher-TESPT compounds doesn't change with different sulfur content.

3.2.4. Intra-cycle elastic and viscous nonlinear response

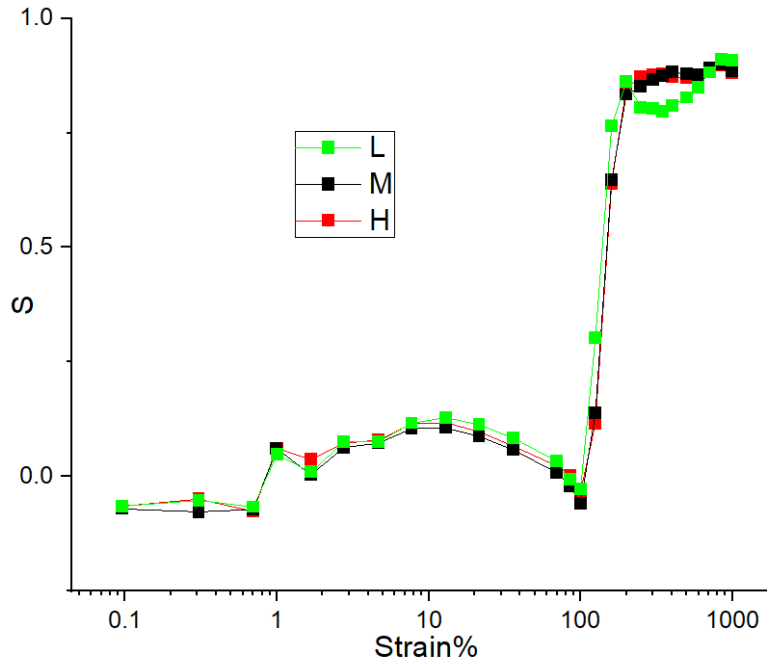

Figure 3.12. Intra-cycle elastic index S pre-cure versus on the strain amplitude showing the dependency on the TESPT content

The evolution of the intra-cycle elastic index S as a function of strain amplitude is shown in Figure 3.12 and provides insight into how the elastic response changes within each oscillation cycle. At very small amplitudes (below approximately 0.7%), S remains slightly negative, reflecting a weak intra-cycle softening influenced by the initial breakage of the weakest filler-filler connections but also by instrumental noise.

When the strain amplitude increases beyond the linear viscoelastic regime, S becomes positive and reaches a local maximum at 13%. This positive value indicates that, within the same oscillation cycle, the slope of the elastic stress-strain curve increases with strain: a signature of intra-cycle strain stiffening. Physically, this response can be attributed to the disruption of the filler network and interfacial chains that deform rather than disentangling [58].

Beyond 13%, S gradually decreases, and as the material approaches the strain (≈ 70-85 %) where the Lissajous loops recover a nearly elliptical shape and G" reaches a minimum, it reaches values close to zero, confirming that the filler-filler network has almost been entirely disrupted and the matrix is still behaving as linear.

As the strain amplitude increases further toward 125-200%, S rises sharply and becomes strongly positive, reaching values around 0.85-0.9. This behaviour coincides with the crossover condition ($G' \approx G''$) and the onset of matrix-dominated deformation,

the marked intra-cycle stiffening in this region simply arises from the stretching of matrix chains [58].

At higher amplitudes, the behaviour of the compounds differs from one another. Comparing the low-TESPT (L) and the high-TESPT formulation (H) it's possible to see that H exhibits constant values and systematically higher than L, that instead decreases at 250%, remains constant until 400% and then increases again, reaching the respective H value only after 700%. This suggests that the stronger filler-rubber coupling in H enhance the elastic resistance within the cycle in this region. After 700% the compounds don't differ anymore.

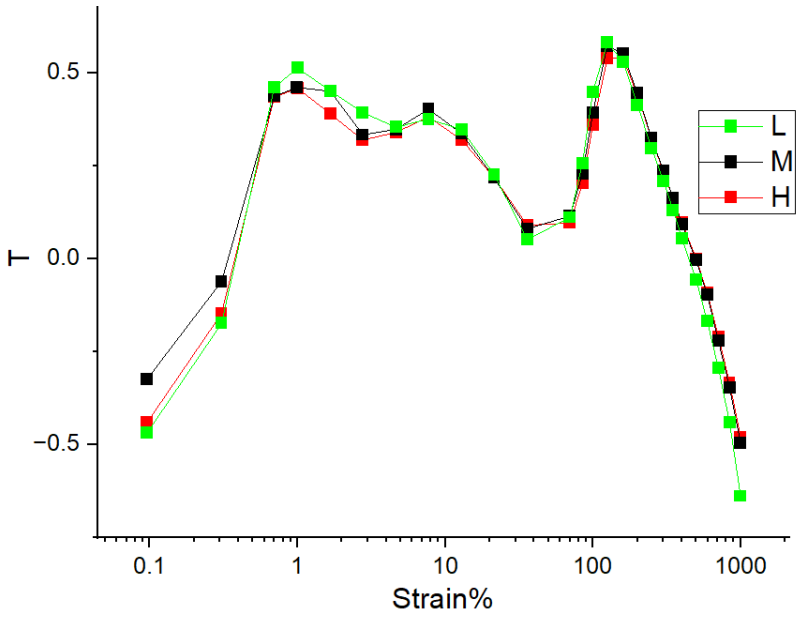

Figure 3.13. Intra-cycle viscous index T pre-cure versus on the strain amplitude showing the dependency on the TESPT content

The evolution of the intra-cycle viscous index T in Figure 3.13 reflects how the dissipative component of the stress changes within each oscillation cycle as the strain amplitude increases.

At the smallest shear strain amplitudes, T assumes slightly negative values, as before probably due to instrumental noise. As the strain amplitude increases, T becomes positive exhibiting two relative maxima, the first located near the onset of nonlinearity and the second, smaller, nearby the previous maximum in S. After these peaks, T gradually decreases and around 35-70% gets close to zero corresponding to the same "neutral" zone as before. Beyond this point, T increases sharply and reaches its absolute maximum at approximately 125%, where tan $\delta \approx 1$. This pronounced rise indicates strong intra-cycle shear thickening, close to the transition from a filler-

controlled to a matrix-controlled regime, consistent with the onset of the matrix-controlled contribution to nonlinearity [59].

At higher amplitudes, T decreases again and beyond roughly 500%, T becomes slightly negative, implying that the viscous component now weakens at large strain rates within the cycle, indicating intra-cycle shear thinning as the oriented polymer chains slide more easily past one another.

Again comparing L and H compounds, the most visible difference is that in the matrix-dominated region after 200% H is constantly higher than L, highlighting the effect of the filler-rubber coupling.

Similarly to what was observed for G' and G", compound M appears to be nearly coincident with H, indicating again that the parameters S and T don't vary proportionally with TESPT content.

3.2.5. Leblanc-Nijman analysis

Table 3.2. Leblanc-Nijman fitting parameters obtained from nonlinear regression of the TTHC-strain curves for each compound pre-cure

Parameter	L	M	H	Lc	Hc
α	0.029	0.027	0.026	0.028201	0.027257
B	0.92	0.063	0.41	0.99	0.62
C	0.0056	0.0057	0.0054	0.0053	0.0051
D	3.7	2.4	3.8	3.1	2.2
TH_m	10.1	12.4	12.8	10.2	11.9

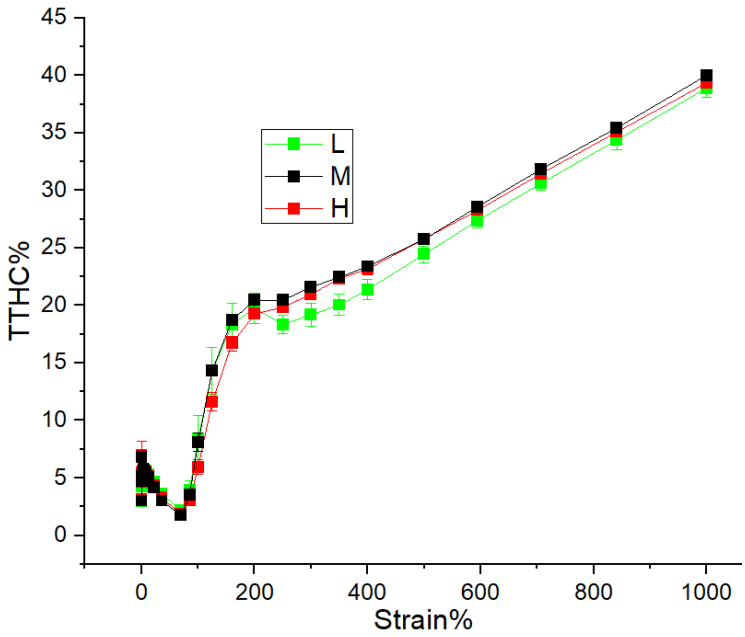

Figure 3.14. TTHC pre-cure versus on the strain amplitude showing the dependency on the TESPT content

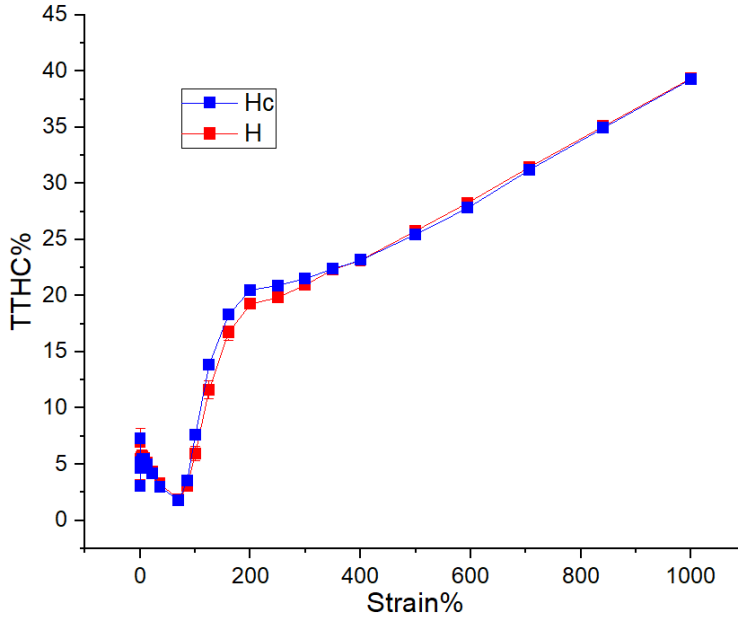

Figure 3.15. TTHC pre-cure versus on the strain amplitude showing the dependency on the sulfur content

While the I_3/I_1 ratio provides a measure of the degree of nonlinearity, and the analysis based on the Chebyshev proposed by Ewoldt give insight into the intracycle behavior of the viscoelastic material, a more comprehensive description of the material response

can be achieved by considering the Total Torque Harmonic Content (TTHC) illustrated in Figure 3.14 and Figure 3.15.

To obtain a quantitative and physically interpretable description, the experimental TTHC curves were fitted using the model proposed by LeBlanc and Nijman, which describes the nonlinear increase of the harmonic content as a function of strain amplitude through five adjustable parameters, illustrated in Table 3.2 decoupling the nonlinear response into two main contributions: an initial term that governs the growth of the harmonic distortion at low strains, the filler response, and a second term that accounts for the high-strain behaviour associated with the polymer response. Since the shape of the experimental TTHC curves differ from the idealized trend originally proposed by LeBlanc, particularly in the low-strain region, where the harmonic content exhibits a decrease between 7.7% and 70% rather than a monotonic increase, the fitting was restricted to the portion of the data corresponding to strain amplitudes above 125%. In this range, the nonlinear response is dominated by the matrix and polymer-filler interactions, and the model adequately reproduces the experimental trend.

The fitted parameters show consistent trends across the different formulations. The parameter α, which controls the initial growth rate of the harmonic content with strain and the final slope of the matrix-dominated part of the graph, follows the order $L > M > H$. Since only data after 125% are considered this indicates that the compound with higher TESPT content exhibits a less steep increase in nonlinearity in the final part of the graph since while the matrix contribution is increasing TTHC, the filler-rubber is becoming less active at higher strains, while for compound L, this does not affect the slope of the graph in its last points since the filler-rubber interaction becomes inactive earlier.

A similar trend is observed for parameter B, which increases the TTHC value for the local maximum at ~ 200% and especially makes the transition less smooth: $B_L > B_M > B_H$. This further confirms that the filler-rubber interactions decrease later for strongly coupled compounds, confirming the dependence of B on the quality of filler dispersion [57].

The parameter C, which defines the strain position of the peak, shows that $C_L > C_H$ and $C_{Lc} > C_{Hc}$ seems to suggest that the maximum contribution of filler-rubber interaction to nonlinearity occurs at higher strains for materials with a more efficient coupling, but C_M presents the highest value among all materials so uncertainty remains about this dependency.

The exponent D, which modulates the slope of the exponential decay, regulating the width of the transition zone, displays irregular variations with no meaningful correlation to TESPT or sulfur content.

Finally, parameter TH_m, which represents the asymptotic value of the harmonic content at large strains, increases with increasing TESPT content ($TH_{m\_L} < TH_{m\_M} <$

TH_{m_H}). This trend is consistent with the higher interfacial coupling efficiency and bound rubber fraction in the high-TESPT compound, which lead to stronger polymer-filler friction and greater harmonic distortion in the matrix-dominated regime.

Comparing the sulfur-adjusted pairs (L vs Lc and H vs Hc); shows higher B values and lower D values both for Lc and Hc, the combination of these effects doesn't significantly alter the shape of the graph, confirming the absence of any difference changing the sulfur content before curing.

3.3. Payne effect in cured compounds

These amplitude sweep tests were performed in the RPA on vulcanized specimens cured under identical conditions for all formulations, with the curing state monitored via the DMA-based analysis described previously; this procedure was adopted to minimize potential variability associated with the curing process.

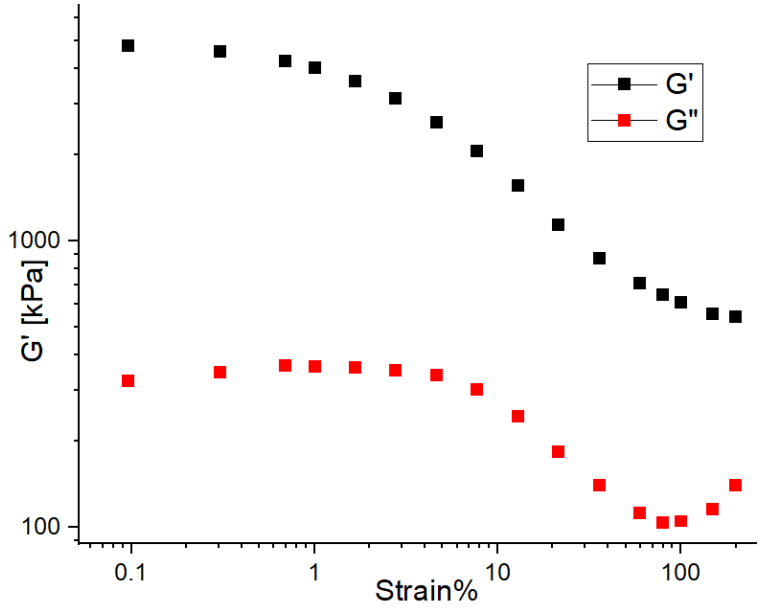

Figure 3.16. Storage (G') and loss (G") modulus in test performed post-cure at $\omega = 0.5Hz$ and $T = 50°C$ for compound M

As previously done for the uncured compounds, examining the evolution of G' and G'' as a function of strain amplitude in Figure 3.16 highlights the main mechanisms governing the material response.

At small strain amplitudes, a first linear viscoelastic plateau can be identified: although G' already decreases slightly from the first points, the variation remains very limited. Once entered in the nonlinear regime, G' decreases significantly as the physical filler-

filler network is progressively destroyed, while simultaneously G″ reaches an absolute maximum just beyond the onset of nonlinearity and then decreases with further strain increase, in a fashion similar to that observed for the uncured compounds.

At high strains, however, a second plateau in G′ emerges, since the physical filler network is almost entirely destroyed and the applied deformation is sustained primarily by the chemical crosslink network, which remains intact within this amplitude range. In contrast, G″ exhibits an absolute minimum around 100% strain, followed by a rapid increase that still remains well below G′ (tan δ < 0.3). This final rise is consistent with nonlinear viscous losses associated with the stretching of polymer chains constrained by chemical crosslinks.

3.3.1. Comparison among cured compounds

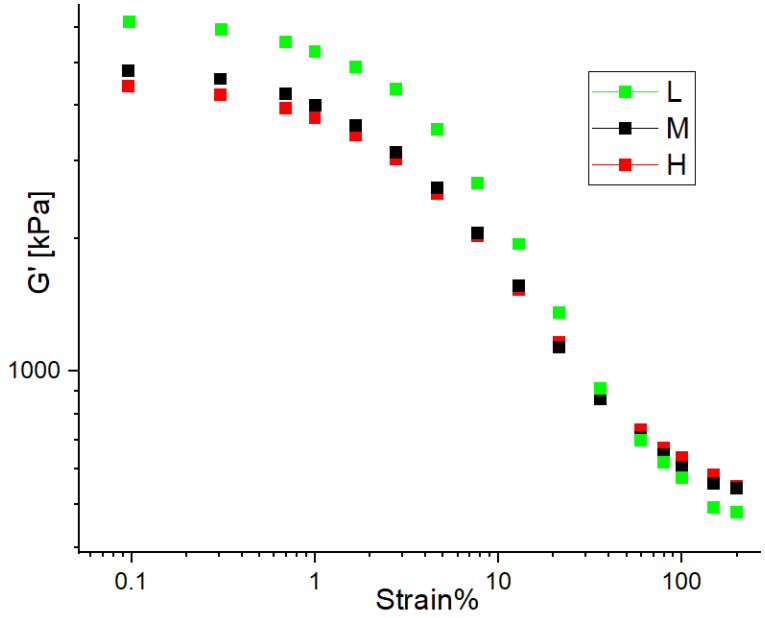

Figure 3.17. Storage modulus G′ post-cure versus on the strain amplitude showing the dependency on the TESPT content

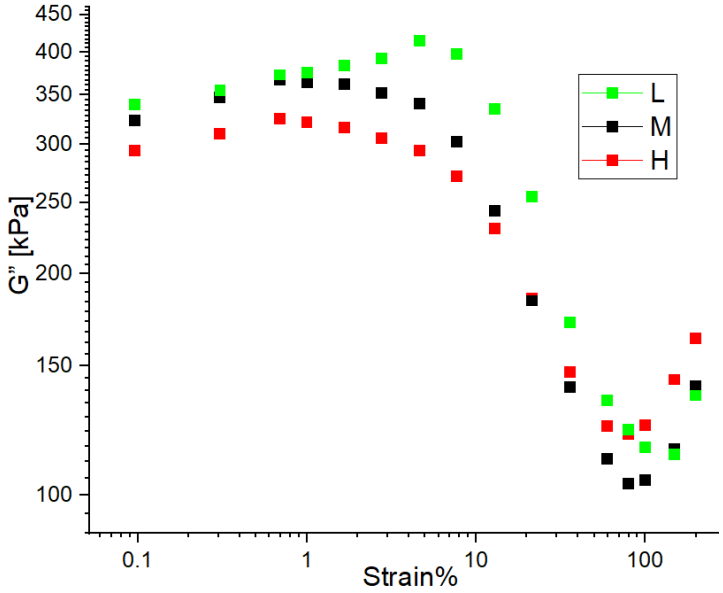

Figure 3.18. Loss modulus G″ post-cure versus on the strain amplitude showing the dependency on the TESPT content

In cured samples, the comparison of G′ and G″ among formulations L, M, and H is shown in Figure 3.17 and Figure 3.18, and reveals distinct trends in the evolution of the storage and loss moduli as a function of strain amplitude.

At small deformations, within the linear region, the ordering $G'(L) > G'(M) > G'(H)$ is observed and reflects the contribution of a stronger physical filler-filler network for lower-TESPT compounds, that still coexists with the permanent chemical crosslink network also after the curing process.

At high amplitudes instead, where G′ reaches a plateau corresponding to the regime where the mechanical response is dominated by the chemical crosslink network, the modulus ordering reverses to $G'(L) < G'(M) < G'(H)$. The higher-TESPT formulation benefits simultaneously from the additional sulfur provided by the coupling agent, which promotes a higher crosslinking degree, and from improved rubber-silica interfacial coupling.

The evolution of the loss modulus G″ confirms this interpretation. At small strains, G″ exhibits a more pronounced maximum for the low-TESPT compound L, occurring at slightly higher deformation, which is consistent with the presence of a larger filler-filler network requiring greater strain to fully activate its dissipative mechanisms.

At high strains, around 150%, G″ reaches an absolute minimum that occurs at slightly lower strain for the high-TESPT compound H. This shift indicates that the chemical network in H is more efficient and denser in crosslinks, entering the dissipative regime earlier. Beyond this minimum, G″ increases again, with H maintaining higher values due to its tighter chemical network and stronger polymer-filler interactions.

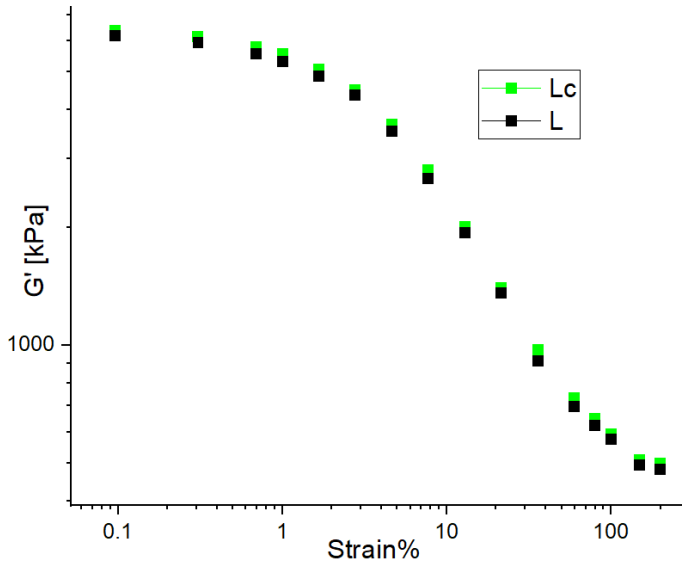

Figure 3.19. Storage modulus G′ post-cure versus on the strain amplitude showing the dependency on the sulfur content for low-TESPT compounds

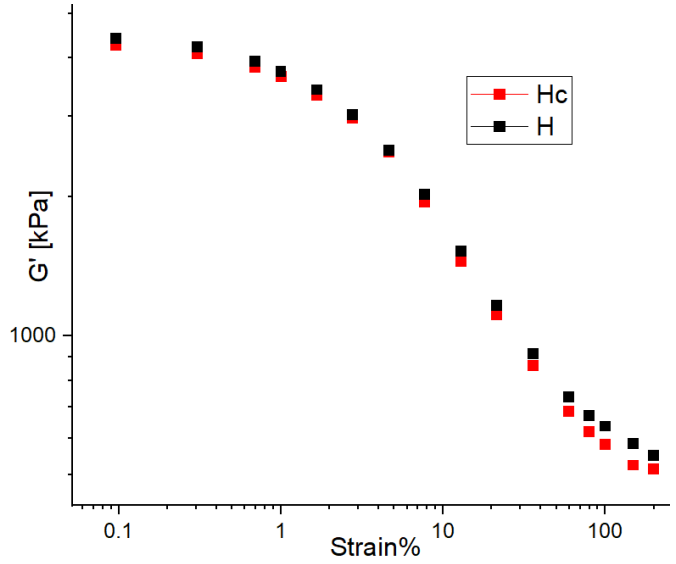

Figure 3.20. Storage modulus G′ post-cure versus on the strain amplitude showing the dependency on the TESPT content for high-TESPT compounds

The comparison of the pairs L-Lc and H-Hc in Figure 3.19 and Figure 3.20 shows that formulations containing more sulfur exhibit slightly higher stiffness across the entire strain range ($G'_{Lc} > G'_{L}$; $G'_{H} > G'_{Hc}$). The difference is small but remains nearly constant throughout the entire domain, appearing as an almost strain-independent vertical shift.

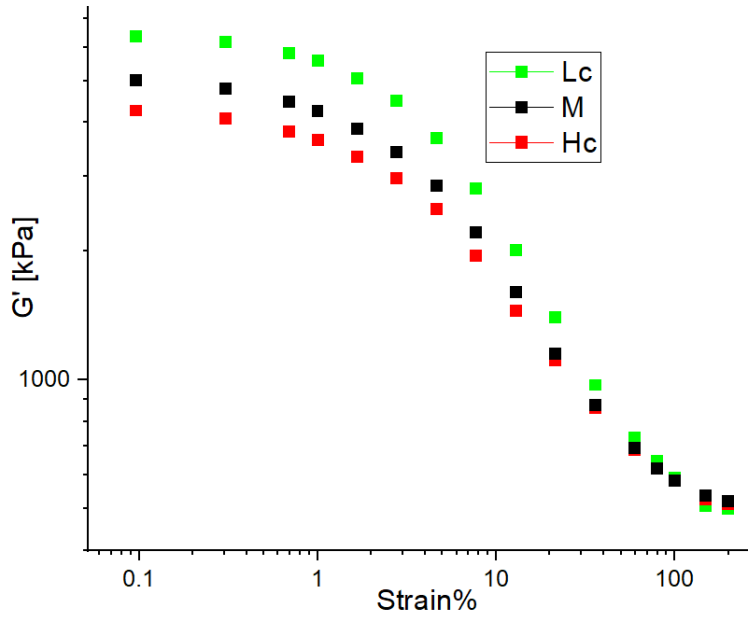

Figure 3.21. Storage modulus G′ post-cure versus on the strain amplitude showing the dependency on the TESPT content for sulfur-balanced compounds

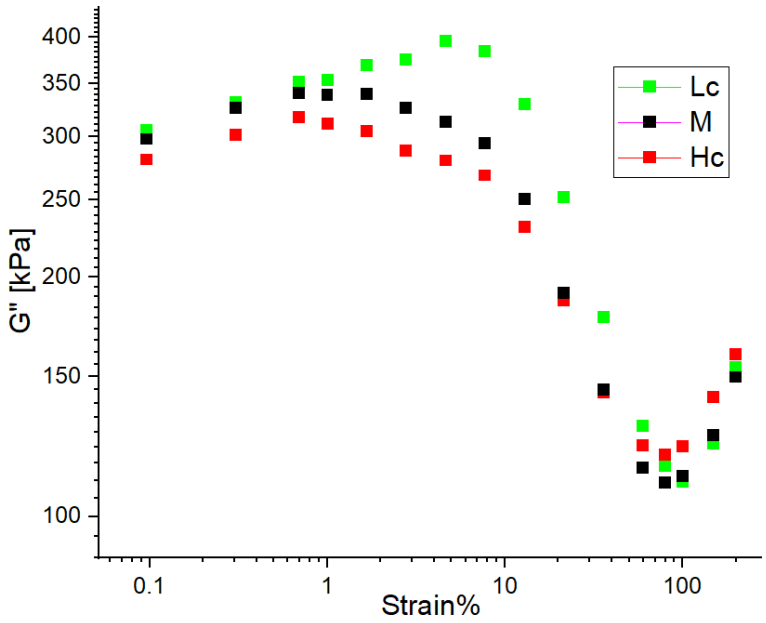

Figure 3.22. Loss modulus G″ post-cure versus on the strain amplitude showing the dependency on the TESPT content for sulfur-balanced compounds

In the sulfur-balanced comparison among Hc, M, and Lc, in Figure 3.21 and Figure 3.22, the low-strain ordering and the softening behaviour remain consistent with the TESPT content, confirming that the physical network dominates the initial regime. However, in the high-amplitude region corresponding to the second plateau of G′, the

curves of all three compounds seems to converge, suggesting that the sulfur adjustment effectively compensates for the TESPT-driven differences in network density.

A closer look at G", though, reveals a subtle but meaningful distinction: the absolute minimum of G" occurs at lower strain for Hc than for Lc, implying that the chemical network in the high-TESPT compound (Hc) becomes active earlier during deformation, consistent with a more efficient crosslink structure. Such behavior further supports the interpretation that TESPT promotes a more effective chemical network, even when the total sulfur level is balanced across formulations.

3.3.2. Qualitative analysis of Lissajous curves

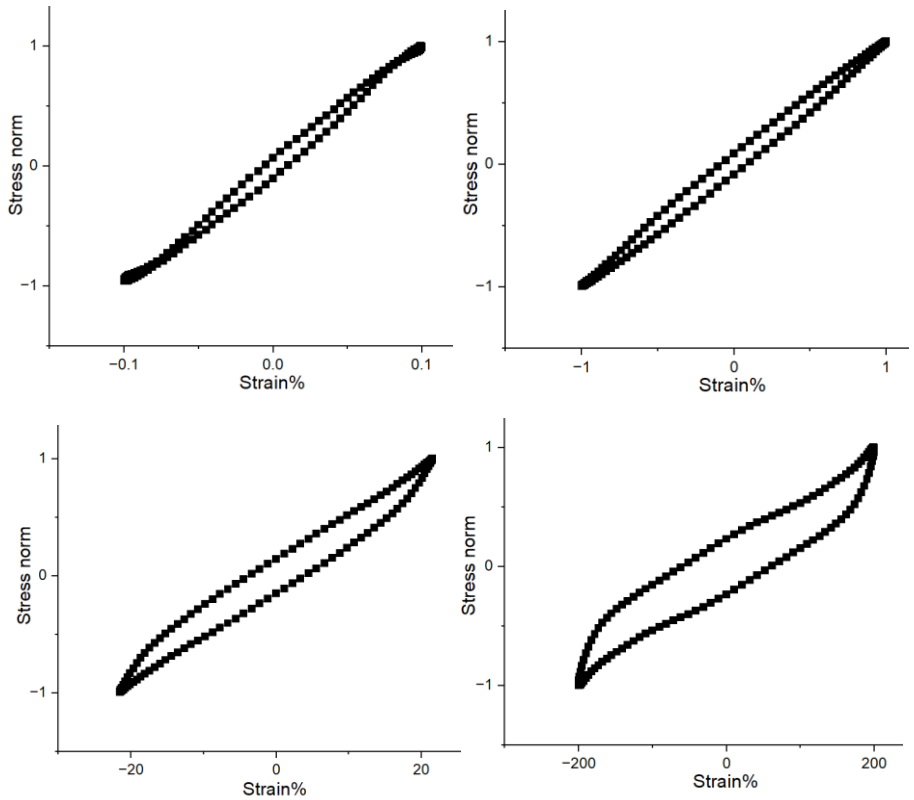

Figure 3.23. Lissajous plots in tests performed post-cure for compound M at strain amplitudes of 0.1% (a), 1% (b), 21.54% (c), 200% (d)

As previously done for the uncured filled rubber, a preliminary qualitative analysis of Lissajous plots (Figure 3.23) is useful to understand how the response evolves with strain amplitude.

At very small strain amplitudes (< 1%, figure 3.23 a), the response is still affected by instrumental noise, which dominates the torque signal at the ends of the ellipse, leading to visible distortions. The most regular elliptical shape is observed at 1%

(figure 3.23 b), although G' already begins to decrease in this region, the waveform remains almost perfectly sinusoidal, indicating that the material is still displaying a predominant linear behaviour.

As the strain amplitude increases, the loops progressively distort and expand, reflecting the activation of nonlinear mechanisms. The distortion becomes clearly visible beyond about 5% and seems to steadily increase with strain (figure 3.23 c and d), consistent with the progressive breakdown of filler clusters.

Visually comparing the different formulations, the low-TESPT compound (L) exhibits smaller loop areas than the high-TESPT compound (H) in the first phase of nonlinearity, but larger loop areas for most of the deformation range (≈ 5-80 %) consistent to what was previously observed in the uncured state. However, the difference may not solely arise from filler morphology, since H also possesses a slightly higher theoretical crosslink density due to the sulfur contribution from TESPT, part of the reduced area in H could be attributed to its more constrained chemical network and consequently to its greater elasticity.

This hypothesis is supported by the sulfur-adjusted comparisons. For both L vs Lc and H vs Hc, the more crosslinked formulation shows slightly smaller loop areas ($Area_L > Area_{Lc}$; $Area_{Hc} > Area_H$), confirming that an increased degree of crosslinking reduces hysteretic dissipation. When comparing compounds with the same nominal sulfur content (Lc, M, Hc), the trend remains dominated by the TESPT level: $Area_{Lc} > Area_{Hc}$ until 60% of strain confirming that the coupling agent plays the major role in controlling nonlinear dissipation through its effect on filler dispersion, making larger areas for lower-TESPT compounds when clusters are breaking, while the influence of sulfur-induced crosslink density is secondary.

3.3.3. Harmonic ratio analysis (I_3/I_1)

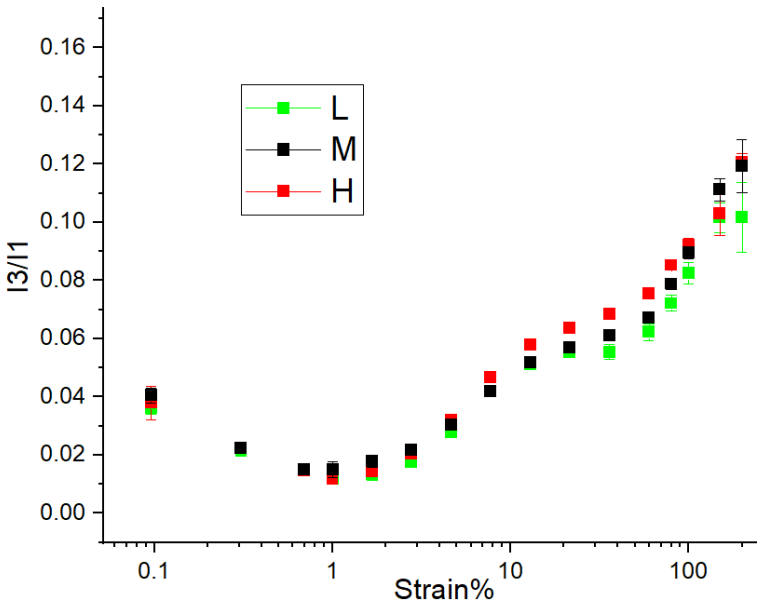

Figure 3.24. Harmonic ratio I_3/I_1 post-cure versus on the strain amplitude showing the dependency on the TESPT content

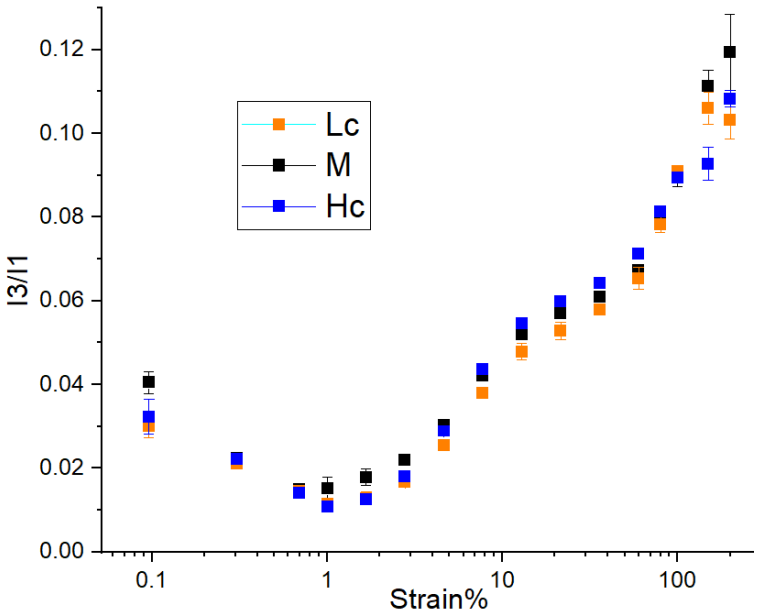

Figure 3.25. Harmonic ratio I_3/I_1 post-cure versus on the strain amplitude showing the dependency on the TESPT content for sulfur-balanced compounds

Figure 3.24 and Figure 3.25 illustrate the evolution of the harmonic ratio I_3/I_1 that confirms the progressive departure from sinusoidal behavior as strain increases. The

first two points show high values due to the already discussed low signal-to-noise ratio and should be not considered. A clear minimum appears at $\gamma \approx 1$ beyond which I_3/I_1 rises steeply up to ~ 13%, consistent with what was observed for the parameter S. From 13% to 60% the ratio continues to increase but with a reduced slope; for some compounds some local maximum can even appear in this range. At larger amplitudes the slope increases slightly again and the curve then grows almost linearly to the maximum applied shear strain amplitude, that could be a signature of the matrix-dominated regime in which the friction of constrained chains governs waveform distortion.

The comparison of the nonlinearity index I_3/I_1 among the cured compounds reveals clear trends that reflect the combined influence of filler-rubber coupling and network structure. From 1% up to about 100%, I_3/I_1 is consistently higher for the high-TESPT compound (H) than for the low-TESPT one (L), indicating that the enhanced silanization promotes earlier distortion of the stress waveform. The more efficient filler-rubber interface in H contributes to a steeper increase, and up to higher strains nonlinearity, while the weaker coupling in L means that this increase in nonlinearity ends for lower strains which makes appear a local maximum at ~ 21%, also present in the S coefficient, marking a more abrupt transition from the filler-dominated regime to the matrix-dominated one.

Beyond 60%, the I_3/I_1 values for L remain lower than those of H, but the rate of increase becomes higher. This suggests that while in the more crosslinked and strongly coupled H compound the chemical network gradually activate, L needs higher strain, leading to a delayed but steeper growth in harmonic content. Beyond 100% the measurements become less reliable due to possible local damage, particularly in L.

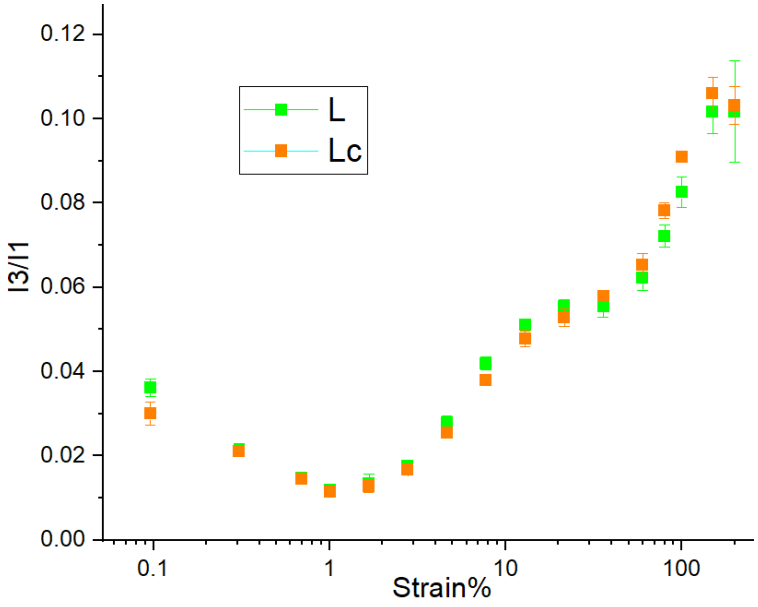

Figure 3.26. Harmonic ratio I_3/I_1 post-cure versus on the strain amplitude showing the dependency on the TESPT content for low-TESPT compounds

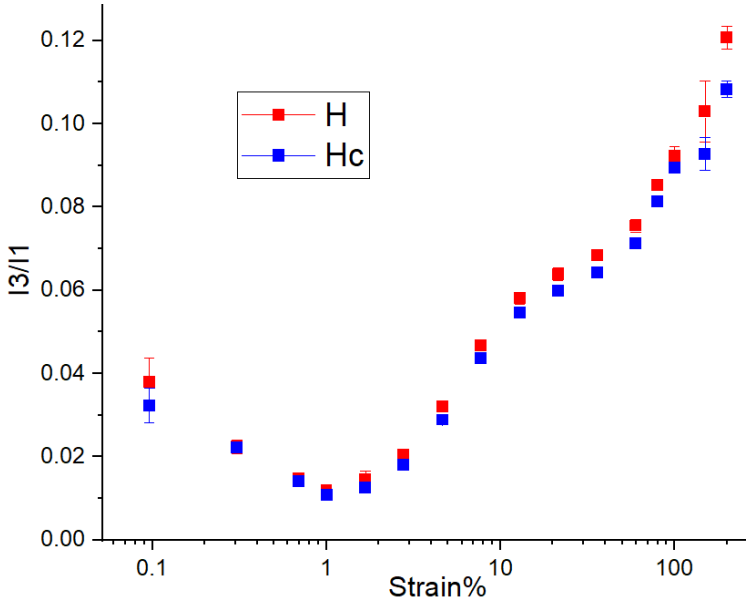

Figure 3.27. Harmonic ratio I_3/I_1 post-cure versus on the strain amplitude showing the dependency on the TESPT content for high-TESPT compounds

The sulfur-adjusted comparisons, in Figure 3.26 and Figure 3.27, further clarify these mechanisms. For the L-Lc pair, the absence of a 21% shoulder in Lc and the smoother slope reduction is similar to the behaviour of the high-TESPT compound, suggesting that the slightly higher crosslink density in Lc stabilizes the transition activating the chemical network earlier. At larger strains (>35 %), I_3/I_1 in Lc exceeds that in L, consistent with the earlier contribution of a denser chemical network. Conversely, the comparison between H and Hc shows no clear difference in slope between 21% and 35

%, implying that for these compounds the transition is made smooth also by the filler-rubber interfacial structure. Overall, these observations confirm that both the degree of silanization and the crosslink density contribute in the transition region.

3.3.4. Intra-cycle elastic and viscous nonlinear response

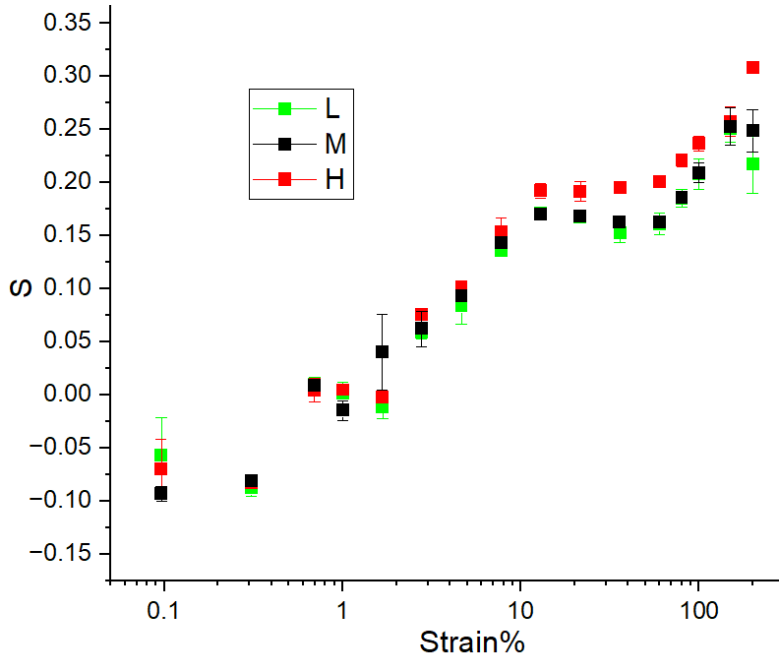

Figure 3.28. Intra-cycle elastic index S post-cure versus on the strain amplitude showing the dependency on the TESPT content

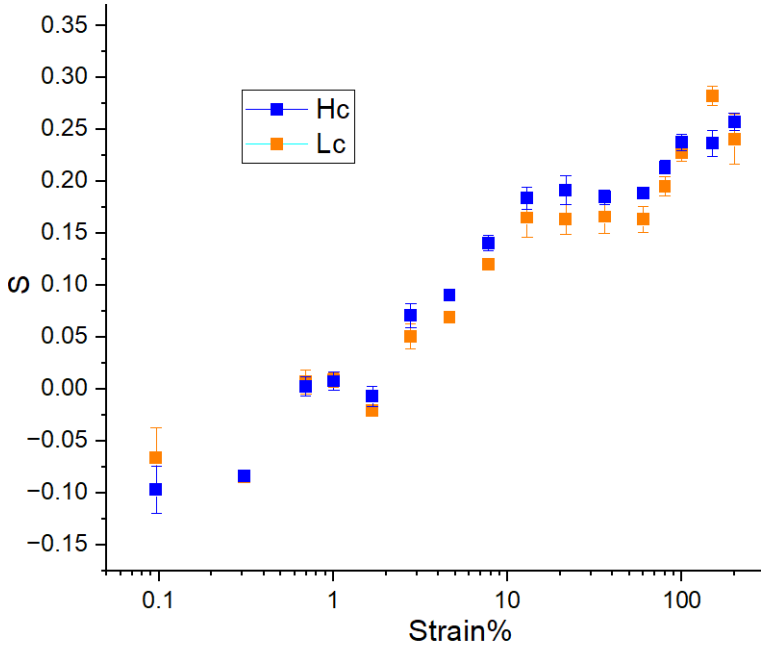

Figure 3.29. Intra-cycle elastic index S post-cure versus on the strain amplitude showing the dependency on the TESPT content for sulfur-balanced compounds

To gain further insight into the intra-cycle elastic behavior of the cured compounds, the Chebyshev coefficient S, shown in Figure 3.28 and Figure 3.29, is evaluated as a function of strain amplitude.

The coefficient is negative at very small amplitudes (0.1-0.3 %), where the response is dominated by instrumental noise, while from 0.7% up to approximately 2%, the values remain close to zero, confirming the quasi-linear viscoelastic behavior of the network despite a decrease of G' in this range, which may be attributed to some sort of rubber relaxation at the constant applied pressure.

Beyond this region, S increases progressively up to around 13%, similarly to what has been observed in the uncured state, but unlike that case, here until roughly 60% S tends to remain constant. At higher amplitudes (≥ 70%), S starts to rise again, increasing almost linearly up to 150%, consistent with progressive strain-stiffening of the crosslinked matrix related to the finite extensibility of the network chains. The values obtained at 200% are less consistent across specimens, some exhibit a further increase while others decrease, but this may be also related to a different degree of damage of the sample which starts breaking in proximity of the grooves of the bi-conical geometry.

The comparison among the cured compounds L, M, and H shows that the differences in the Chebyshev coefficient S become significant only beyond approximately 2%, when the response departs from the linear regime. In this range, a clear ordering is observed, with $S_L < S_M < S_H$. The higher values of S in the high-TESPT compound reflect mainly its stronger interfacial coupling, which enhances the effective stiffness

of the filler-rubber interface and promotes earlier intra-cycle strain stiffening. The fact that $S_{Lc} < S_{Hc}$, suggest that even if the sulfur content has some influence, it's secondary.

In the intermediate range (≈ 30-60 %) the difference among formulations becomes more evident. L and M exhibit a maximum followed by a limited decrease, H display less pronounced variations; while despite $S_{Lc} < S_{Hc}$, the behaviour is very similar in this case. This suggests that a greater quantity of TESPT increases the intra-cycle strain hardening as it promotes stronger interfacial constraints, while the crosslinking density controls the general dependence of the S parameter on strain.

At higher amplitudes, the trend $S_L < S_M < S_H$ persists up to about 150%, where all compounds converge to similar values, while interestingly, at 200%, the three compounds diverge again: H continues to increase, M remains roughly constant, and L shows a noticeable drop. This behaviour could mark the onset of network damage in L, whose weaker filler-rubber interface and lower crosslink density make it more prone to damage, meanwhile, the more efficiently coupled compound H can sustain further strain stiffening.

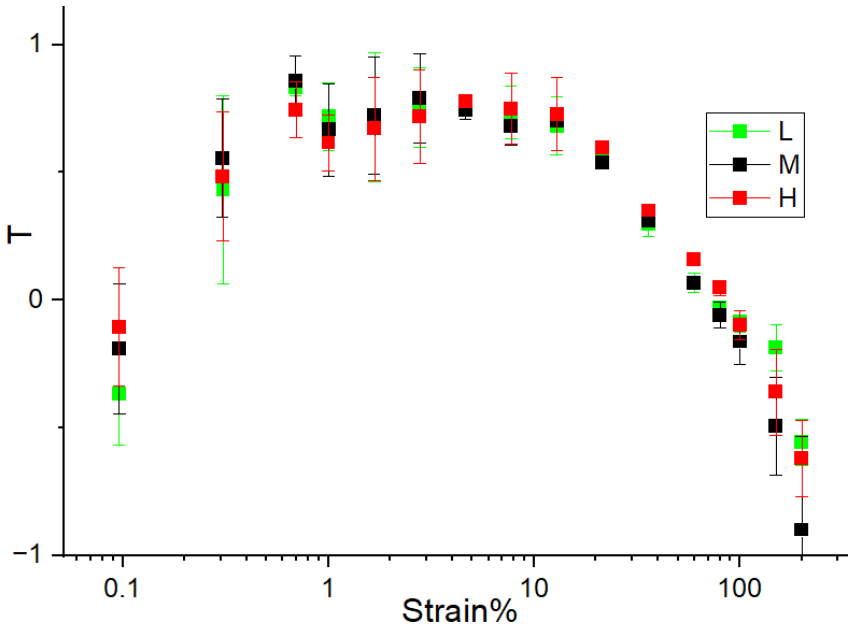

Figure 3.30. Intra-cycle viscous index T post-cure versus on the strain amplitude showing the dependency on the TESPT content

The Chebyshev coefficient T, in Figure 3.30, is evaluated to describe the intra-cycle behaviour of the viscous components of the cured compounds, providing complementary information to the elastic coefficient S.

The initial points at 0.1% and 0.3% should not be considered due to instrumental noise which is reflected in the causes a relatively large standard deviations.

At 0.7% T exhibits an initial local maximum, when weak bonds begin to break, then after a minimum at 1%, the coefficient increases again, reaching a second and broader maximum at approximately 5%, when the breakage of weak filler-filler networks might be the governing phenomenon, as it was in the case of the uncured rubber.

Beyond this point, T decreases monotonically up to the highest strains investigated, differing from the uncured rubber case in that there is no increase after 70%, probably due to the elastic contribution presence of the crosslinked matrix. Around 100%, T crosses zero and becomes negative, implying a transition to a shear-thinning behavior dominated by the aligning of the chemical network.

The cured formulations shows similar values of the parameter T until 21%, beyond that, $T_H > T_L$ up to about 100%. The more efficient coupling in H stabilizes the filler-rubber interface that seems to dominate the filled rubber behaviour in this region. At larger strains (>100 %), the order reverses ($T_H < T_L$ but having negative values, $|T_H| > |T_L|$).

3.3.5. TTHC and Leblanc-Nijman parameters analysis

Table 3.3. Leblanc-Nijman fitting parameters obtained from nonlinear regression of the TTHC-strain curves for each compound post-cure

Parameter	L	M	H	Lc	Hc
α	0.061	0.064	0.063	0.063	0.063
B	1.98	1.92	1.90	1.72	1.90
C	0.037	0.036	0.034	0.037	0.035
D	1.65	1.68	1.67	1.68	1.70
TH_m	7.0	7.9	8.7	7.9	8.1

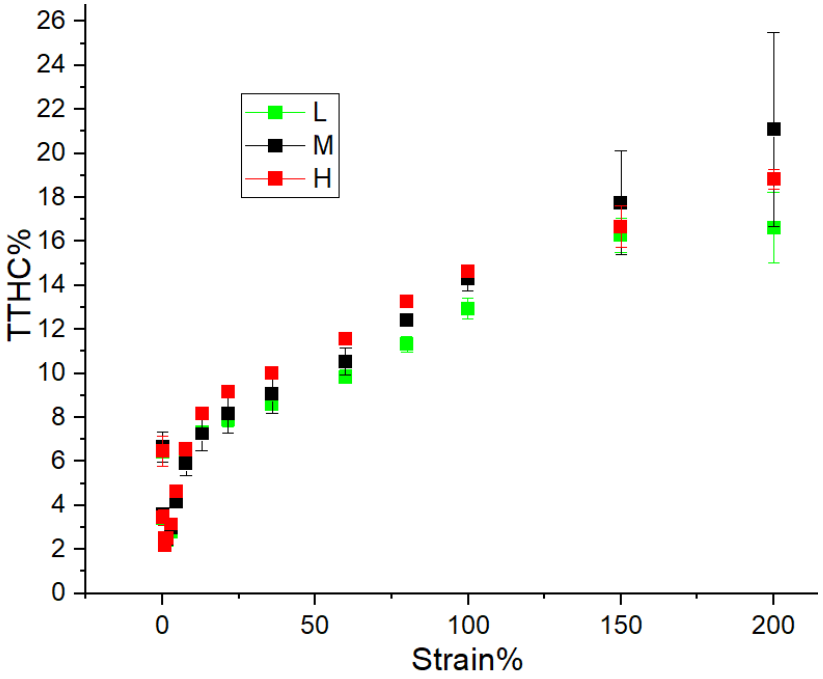

Figure 3.31. TTHC post-cure versus on the strain amplitude showing the dependency on the TESPT content

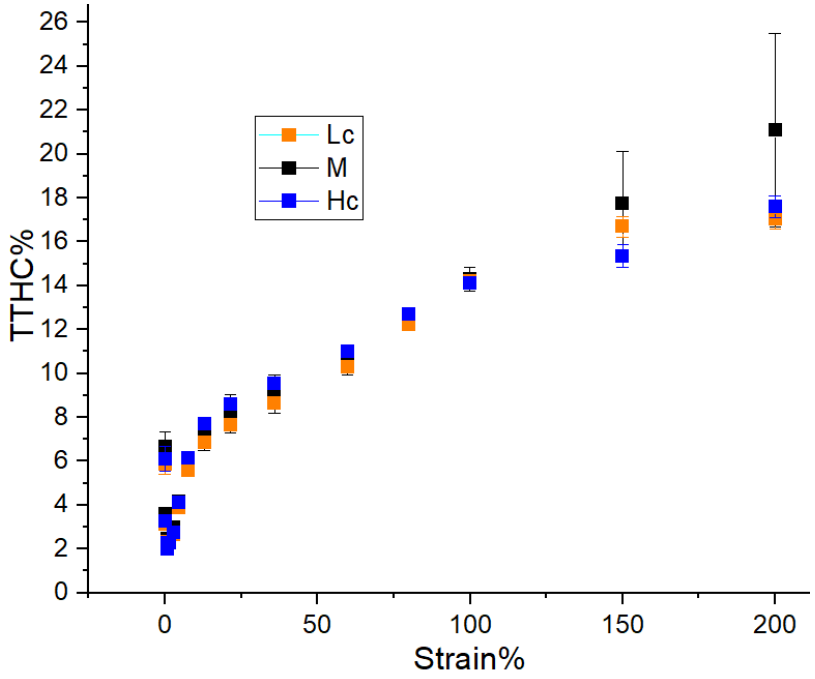

Figure 3.32. TTHC post-cure versus on the strain amplitude showing the dependency on the TESPT content for sulfur-balanced compounds

Contrary to what was done for the uncured systems, in this case the cured compounds exhibit TTHC curves, illustrated in Figure 3.31 and Figure 3.32, that are well captured by the LeBlanc-Nijman model over almost the full strain range, specifically from 1.67% to 100%, indicating that the model can successfully reproduce the evolution of nonlinearity in these crosslinked materials. In this context, the fitting parameters, shown in Table 3.3, acquire a slightly different physical meaning: they now describe the balance between the progressive breakdown of the filler-filler structure, the interfacial interactions between the rubber matrix and the filler surface and the elastic response of the chemical network.

Parameter α, which controls the initial rise the total harmonic content, remains nearly constant across formulations, reflecting a comparable activation rate of nonlinearity in the early stages of deformation. The parameter B follows the same trend observed in the uncured compounds ($B_L > B_M > B_H$), indicating that even after cure, the lower-TESPT materials retain a higher degree of interfacial heterogeneity [57].

Parameter C increases with decreasing TESPT content ($C_L > C_M > C_H$ and $C_{Lc} > C_{Hc}$), indicating that the transition to matrix-dominated behavior occurs at lower strain for poorly coupled systems, where higher silanized systems stabilizes the filler-rubber network until higher strains.

Parameter D slightly increases for higher-TESPT compounds, showing a narrower transition region. In low-TESPT compounds, the heterogeneous cluster structure leads to a broader, more gradual disintegration.

The most meaningful result is provided by parameter TH_m, which exhibits $TH_{m\_L} < TH_{m\_M} < TH_{m\_H}$, while TH_{m_Hc} is only slightly higher than TH_{m_Lc}. In this regime, the parameter E increases markedly with the total sulfur content, confirming its correlation with the chemical crosslink density and the stiffness of the cured network. A smaller yet consistent increase is also observed with higher TESPT levels (at constant sulfur), which can be attributed to the residual contribution of the filler-rubber coupling.

Overall, extending the LeBlanc-Nijman model to cured compounds in this strain range confirms its ability to describe the experimentally observed behaviour and highlights how its parameters can serve as practical indicators of network stiffness, interfacial efficiency, and structural heterogeneity, even beyond the original uncured formulation.

3.4. Further considerations about the compound with the intermediate-TESPT content

Across the different experimental analyses, the formulation containing an intermediate amount of TESPT (M) consistently does not position itself halfway between the low-TESPT (L) and the high-TESPT (H) compounds.

In the curing kinetics M follows the expected order $H > M > L$, however its curing rate remains noticeably closer to L than to H, indicating that the TESPT effect is not linear over the investigated concentration range.

In contrast, in the uncured state M, G' and G'' of M are generally closer to H than to L, especially within the linear viscoelastic region and in the early nonlinear regime. The same tendency is confirmed if the Chebyshev analysis parameters (S and T) are considered: also in this case M often approaches H, to the point of overlapping in some strain ranges. This indicates that after a certain threshold, the increase in TESPT content seem not to affect the filler-filler and filler-rubber interaction.

In the cured state, G' of M is still similar to that of L at low shear strains. In the intermediate shear strain range, the analysis based both on the Chebyshev elastic parameter S and on the harmonic ratio I_3/I_1, show that at a given shear strain the values of the parameters for M get closer to that for L When sulfur-balanced formulations (L_c and H_c) are considered instead, the position of M is less shifted towards one extreme, suggesting that part of the deviation in the previous comparison arises from the sulfur contribution to crosslink density.

Again, these observations indicate that the dependence of the nonlinear viscoelastic response on TESPT content is not simply linear.

3.5. Effect of Normal Pressure on the Nonlinear Viscoelastic Response

The Payne effect is usually investigated at atmospheric pressure. This is the case of dynamic mechanical analysis, in torsion, shear or tension. However in RPA the use of the closed chamber implies that the sample is pressurized. Up to this point, RPA was operated always at the same pressure, and given the same curing history was applied to all the materials, which compositional difference were limited we can assume that pressure was the same in all tests. One of the RPA available for the research allowed to control the pressure in different levels. Therefore, the amplitude sweep tests were performed on cured samples at three different normal pressures (580psi, 760psi, and 1000psi) . Results show clear differences in the viscoelastic response; increasing the applied pressure seem to give a more accurate representation of the material behavior, as artefacts associated with wall slip and incomplete confinement are progressively suppressed.

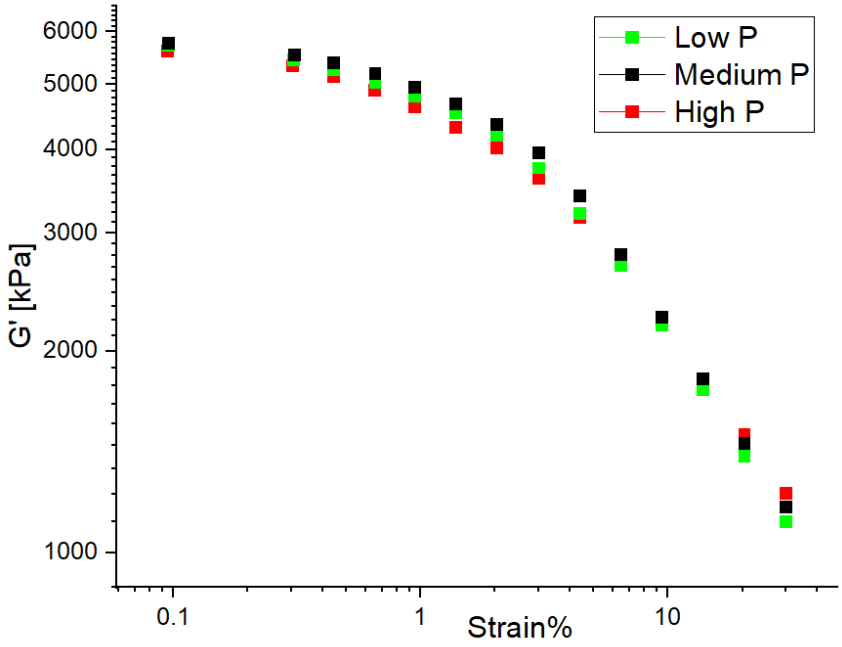

Figure 3.33. Storage modulus G′ post-cure versus on the strain amplitude showing the dependency on the normal pressure for compound Lc

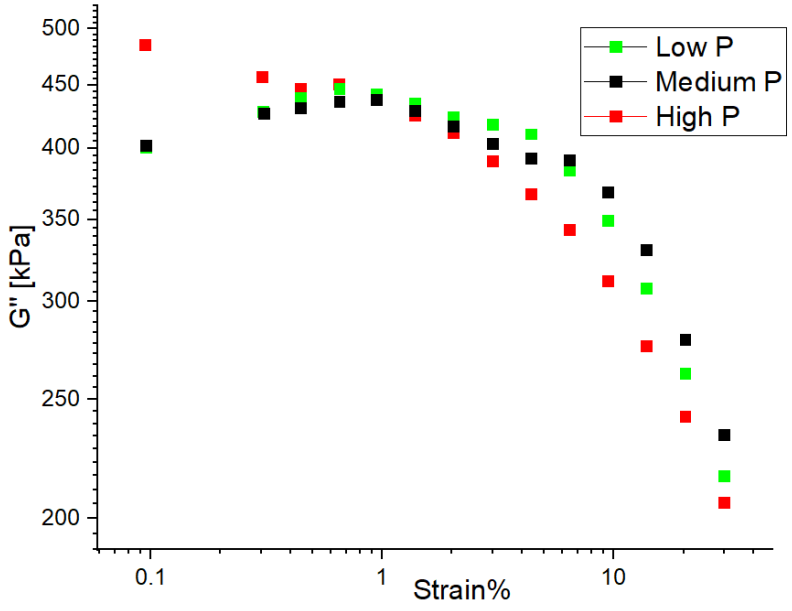

Figure 3.34. Loss modulus G″ post-cure versus on the strain amplitude showing the dependency on the normal pressure for compound Lc

Figure 3.33 and Figure 3.34 illustrate G′ and G″. Visually it can be observed that at low pressure, the decay of G′ between 0.1% and 30% strain is larger while at high pressure the softening is reduced. In parallel, G″ at high pressure is constantly lower than the other two cases for strains greater than 1%, showing that it effectively suppresses wall

slip. The fact that G″ measured at medium pressure after 6% of strain is higher than that at low pressure could suggest that the medium pressure is still insufficient to effectively suppress wall slip, but it's enough to increase internal friction between molecules.

Overall, the comparison demonstrates that increasing normal pressure eliminates artefacts related to wall slip. However, the effect of pressure itself would require an extensive investigation which is out of the scope of the present work.

4 Conclusion and Future Developments

This work has investigated the influence of TESPT content and sulfur level on the curing kinetics and nonlinear viscoelastic behaviour of silica-filled SBR compounds, combining conventional dynamic analysis with harmonic-based approaches such as I_3/I_1, Chebyshev coefficients, and the LeBlanc-Nijman model applied to the total torque harmonic content (TTHC).

The curing kinetics clearly indicate that TESPT is the dominant parameter controlling network formation. The trend $H > M > L$ confirms that increasing TESPT accelerates vulcanization, consistent with its dual role as sulfur donor and coupling agent. In contrast, small variations in elemental sulfur alone produce only minor changes in curing rate.

In the uncured state, the nonlinear response is governed by the progressive breakdown of the filler-filler network. The amplitude sweep and harmonic analyses consistently show a more pronounced Payne effect in the low-TESPT compound, characterized by higher initial stiffness and stronger modulus softening. At larger strain amplitudes, however, the differences among formulations progressively decrease when the response becomes matrix-dominated, with only minor residual distinctions between compounds.

After vulcanization, the mechanical response reflects the combined action of the residual filler structure, filler-rubber interactions, and the chemical crosslink network. At small strains, the modulus ordering still mirrors the contribution of the physical filler network, whereas at high strains the second G′ plateau highlights the dominance of the chemical network. Importantly, when sulfur-balanced formulations are compared, the differences among compounds in the high-strain regime are significantly reduced. This result indicates that TESPT mainly influences the low-strain response and interfacial efficiency, without introducing major advantages at large deformation.

The pressure-dependent tests demonstrate that increasing normal pressure progressively suppresses wall-slip artefacts and reveals a more intrinsic material behaviour.

An interesting observation concerns the intermediate formulation M, whose behavior does not always scale linearly between L and H. Across different nonlinear indicators, M sometimes approaches one extreme more closely than expected overlapping at times, suggesting that the reinforcement efficiency of TESPT may not increase proportionally with concentration within the investigated range and could reach a saturation level where a further TESPT increase is completely inefficient if not harmful.

Future developments could therefore explore formulations with higher TESPT contents to verify the possible existence of a saturation level, as well as wider variations in sulfur concentration to further decouple the respective contributions of chemical crosslink density and filler-rubber coupling.

Bibliography

[1] B. Erman, J. E. Mark and C. M. Roland, The Science and Technology of Rubber, Oxford: Elsevier, 2013.

[2] J. Ciambella, Experimental Testing and Nonlinear Viscoelastic Modeling of Filled Rubber, Roma, 2010.

[3] W. D. Callister, Materials Science and Engineering, John Wiley & Sons, 2007.

[4] V. Silva, R. Nunes, A. Sousa, Epoxidized natural rubber and hydrotalcite compounds: rheological and thermal characterization, 2017.

[5] M. Masłowski, J. Miedzianowska, K. Strzelec, The potential application of cereal straw as a bio-filler for elastomer composites, 2020.

[6] A. Nihmath, M. Ramesan, Hydroxyapatite as a Potential Nanofiller in Technologically Useful Chlorinated Acrylonitrile Butadiene Rubber, 2020.

[7] B. Szadkowski, A. Marzec, P. Rybiński, W. Żukowski, M. Zaborski, Characterization of Ethylene–propylene Composites Filled with Perlite and Vermiculite Minerals: Mechanical, Barrier, and Flammability Properties, 2020.

[8] I. Ulfah, R. Fidyaningsih, S. Rahayu, D. Fitriani, D. Saputra, D. Winarto, L. Wisojodharmo, Influence of Carbon Black and Silica Filler on the Rheological and Mechanical Properties of Natural Rubber Compound, 2015.

[9] G. Heinrich, M. Klüppel , T. Vilgis, Reinforcement of elastomers, 2002.

[10] A. Sowińska-Baranowska, M. Maciejewska, Influence of the Silica Specific Surface Area and Ionic Liquids on the Curing Characteristics and Performance of Styrene–Butadiene Rubber Composites, 2021.

[11] C. Zhang, Z. Tang, B. Guo, L. Zhang, Concurrently improved dispersion and interfacial interaction in rubber/nanosilica composites via efficient hydrosilane functionalization, 2019.

[12] C. Zhang, Z. Tang, B. Guo, L. Zhang, Significantly improved rubber-silica interface via subtly controlling surface chemistry of silica, 2018.

[13] N. Noriman, H. Ismail, Properties of styrene butadiene rubber (SBR)/recycled acrylonitrile butadiene rubber (NBRr) blends: The effects of carbon black/silica (CB/Sil) hybrid filler and silane coupling agent, Si69, 2012.

[14] A. Kosmalska, M. Zaborski, L. Ślusarski, Adsorption of curatives and activity of silica toward elastomers, 2003.

[15] N. Rattanasom, T. Saowapark, C. Deeprasertkul, Reinforcement of natural rubber with silica/carbon black hybrid filler, 2007.

[16] M. Maciejewska, A. Sowińska, Influence of Fillers and Ionic Liquids on the Crosslinking and Performance of Natural Rubber Biocomposites, 2021.

[17] M. Maciejewska, M. Zaborski, Ionic Liquids Applied to Improve the Dispersion of Coagent Particles in an Elastomer, 2013.

[18] A. Sowińska, M. Maciejewska, L. Guo, E. Delebecq, Effect of SILPs on the Vulcanization and Properties of Ethylene–Propylene–Diene Elastomer, 2020.

[19] M. Castellano, L. Conzatti, G. Costa, L. Falqui, A. Turturro, B. Valenti, F. Negroni, Surface modification of silica: Thermodynamic aspects and effect on elastomer reinforcement, 2005.

[20] G. Mathew, M. Huh, J. Rhee, M. Lee, C. Nah, Improvement of properties of silica-filled styrene-butadiene rubber composites through plasma surface modification of silica, 2004.

[21] B. Guo, F. Chen, Y. Lei, W. Chen, Significantly improved performance of rubber/silica composites by addition of sorbic acid, 2010.

[22] I. Mora-Barrantes, A. Rodríguez, L. Ibarra, L. González, J. Valentín, Overcoming the disadvantages of fumed silica as filler in elastomer composites, 2011.

[23] G. Allegra, G. Raos, M. Vacatello, Theories and simulations of polymer-based nanocomposites: From chain statistics to reinforcement, 2008.

[24] L. Huang, F. Yu, Y. Liu, A. Lu, Z. Song, W. Liu, Y. Xiong, H. He, S. Li, X. Zhao, S. Cui, C. Zhu, Structural analyses of the bound rubber in silica-filled silicone rubber nanocomposites reveal mechanisms of filler-rubber interaction, 2023.

[25] Y. Yue, H. Zhang, Z. Zhang, Y. Chen, Polymer–filler interaction of fumed silica filled polydimethylsiloxane investigated by bound rubber, 2013.

[26] C. Tian, G. Chu, Y. Feng, Y. Lu, C. Miao, N. Ning, L. Zhang, M. Tian, Quantitatively identify and understand the interphase of SiO2/rubber nanocomposites by using nanomechanical mapping technique of AFM, 2019.

[27] L. Hall, A. Jayaraman, K. Schweizer, Molecular theories of polymer nanocomposites, 2010.

[28] Rheometrics System Analyzer RSAIII user manual, 2005.

[29] TA Instruments, Rheology Theory and Applications.

[30] S. N. Ganeriwala and C. A. Rotz, "Fourier transform mechanical analysis for determining the nonlinear viscoelastic properties of polymers," Polymer Engineering & Science, vol. 27, no. 2, pp. 165-178, 1987.

[31] C. G. Robertson and X. Wang, "Spectral hole burning to probe the nature of unjamming (Payne effect) in particle-filled elastomers," Europhys. Lett., vol. 76, no. 2, pp. 278-284, 2006.

[32] L. Chazeau, J. D. Brown, L. C. Yanko and S. S. Sternstein, "Modulus Recovery Kinetics and Other Insights Into the Payne Effect for Filled Elastomers," Center for Composite Materials and Structures Rensselaer Polytechnic Institute, Troy, New York, 2000.

[33] G. Heinrich and M. Klüppel, "Recent Advances in the Theory of Filler Networking in Elastomers," in Filled Elastomers Drug Delivery Systems , 2002, pp. 1-44.

[34] C. G. R. Amy M Randall, "Linear-nonlinear dichotomy of the rheological response of particle-filled polymers," Journal of Applied Polymer Science, vol. 131, no. 19, 2014.

[35] J. L. Leblanc, "Large amplitude oscillatory shear experiments to investigate the nonlinear viscoelastic properties of highly loaded carbon black rubber compounds without curatives," Journal of Applied Polymer Science, vol. 1090, no. 2, pp. 1271-1293, 2008.

[36] K. Atalık, R. Keunings, On the occurrence of even harmonics in the shear stress response of viscoelastic fluids in large amplitude oscillatory shear, 2004.

[37] M. Graham, Wall slip and the nonlinear dynamics of large amplitude oscillatory shear flows, 1995.

[38] S. Kallus, N. Willenbacher, S. Kirsch, D. Distler, T. Neidhöfer, M. Wilhelm, H. Spiess, Characterization of polymer dispersions by Fourier transform rheology, 2001.

[39] R. Ewoldt, A. Hosoi, G. McKinley, New measures for characterizing nonlinear viscoelasticity in large amplitude oscillatory shear, 2008.

[40] K. Cho, K. Hyun, K. Ahn, S. Lee, A geometrical interpretation of large amplitude oscillatory shear response, 2005.

[41] R. Ewoldt, P. Winter, J. Maxey, G. McKinley, Large amplitude oscillatory shear of pseudoplastic and elastoviscoplastic materials, 2010.

[42] A. Payne, The dynamic properties of carbon black-loaded natural rubber vulcanizates. Part I, 1962.

[43] A. Payne, A note on the existence of a yield point in the dynamic modulus of loaded vulcanizates, 1960.

[44] A. Meera, S. Said, Y. Grohens, S. Thomas, Nonlinear Viscoelastic Behavior of Silica-Filled Natural Rubber Nanocomposites, 2009.

[45] J. Leblanc, Simplified modeling calculations to enlighten the mechanical properties (modulus) of carbon black filled diene rubber compounds, 2011.

[46] D. Zhao, S. Ge, E. Senses, P. Akcora, J. Jestin, S. Kumar, Role of Filler Shape and Connectivity on the Viscoelastic Behavior in Polymer Nanocomposites, 2015.

[47] Y. chen, C. Xu, Specific nonlinear viscoelasticity behaviors of natural rubber and zinc dimethacrylate composites due to multi-crosslinking bond interaction by using rubber process analyzer 2000, 2011.

[48] W. Zhou, L. Chen, J. Lu, Z. Qi, N. Huang, L. Li, W. Huang, Imaging the strain induced carbon black filler network structure breakage with nano X-ray tomography, 2014.

[49] S. Sternstein, A. Zhu, Reinforcement Mechanism of Nanofilled Polymer Melts As Elucidated by Nonlinear Viscoelastic Behavior, 2002.

[50] V. Sridhar, R. Choudhary, D. Tripathy, Effect of carbon blacks on relaxation phenomenon of chlorobutyl vulcanizates, 2006.

[51] K. Stöckelhuber, A. Svistkov, A. Pelevin, G. Heinrich, Impact of Filler Surface Modification on Large Scale Mechanics of Styrene Butadiene/Silica Rubber Composites, 2011.

[52] M. Aranguren, E. Mora, J. DeGroot, C. Macosko, Effect of reinforcing fillers on the rheology of polymer melts, 1992.

[53] J. Ramier, C. Gauthier, L. Chazeau, L. Stelandre, L. Guy, Payne effect in silica-filled styrene–butadiene rubber: Influence of surface treatment, 2007.

[54] S. Merabia, P. Sotta, D. Long, A Microscopic Model for the Reinforcement and the Nonlinear Behavior of Filled Elastomers and Thermoplastic Elastomers (Payne and Mullins Effects), 2008.

[55] H. Montes, F. Lequeux, J. Berriot, Influence of the Glass Transition Temperature Gradient on the Nonlinear Viscoelastic Behavior in Reinforced Elastomers, 2003.

[56] H. Montes, T. Chaussée, A. Papon, F. Lequeux, L. Guy, Particles in model filled rubber: Dispersion and mechanical properties, 2010.

[57] J. Leblanc, G. Nijman, Engineering performance and material viscoelastic analyses along a compounding line for silica-based compounds, part 2: Nonlinear viscoelastic analysis, 2009.

[58] S. Yang, P. Akcora, Deformation of Chemically Heterogeneous Interfacial Layers of Polymer Nanocomposites, 2019

[59] S. Coppola, M. Demaio, A.G. Solito, L. Franchini, Large Amplitude Oscillatory Shear of filled rubber: an essential tool to characterize rubber/filler interactions, 2022

List of Figures

List of Tables